SPIE.SPOTLIGHT

Advanced Sensing with Micro-optical Whispering-Gallery-Mode Resonators

Giancarlo C. Righini
and Silvia Soria

Advanced Sensing with Micro-optical Whispering-Gallery-Mode Resonators

by Giancarlo C. Righini and Silvia Soria

doi: http://dx.doi.org/10.1117/3.2272482
PDF ISBN: 9781510610880
epub ISBN: 9781510610897
mobi ISBN: 9781510610903

Published by

SPIE Press
P.O. Box 10
Bellingham, Washington 98227-0010 USA
Phone: +1 360.676.3290
Fax: +1 360.647.1445
Email: Books@spie.org
Web: http://spie.org

Spotlight vol. SL28
Last updated: 31 March 2017

SPIE.

Table of Contents

SPIE Spotlight Series

Welcome to SPIE Spotlight eBooks! This series of tutorials is designed to educate readers about a wide range of topics in optics and photonics. I like to think that these books address subjects that are too broad for journal articles but too concise for textbooks. We hope you enjoy this eBook, and we encourage you to submit your ideas for future Spotlights online.

Robert D. Fiete, *Series Editor*
Harris Corp.

Editorial Board

Preface

Whispering gallery mode (WGM) resonators have enabled real-world sensing applications by measuring physical quantities, such as temperature, mass, and pressure, as well as chemical and biomedical parameters. In the latter context, important achievements, such as label-free detection of a single virus, single molecules, and large objects, such as bacteria, have been recorded. We try to provide a quick overview of the state of the art of WGM-based sensors. A summary of the fundamental principles, the mathematical theory, and the main properties of different types of such resonators is also given.

1 Introduction

The number of sensor applications is steadily growing, and new application areas are opening as well, confirming that the ability to accurately sense physical, chemical, or biological parameters is of paramount importance for science, engineering, and biomedicine. In parallel, sensor technologies are improving in terms of accuracy, reliability, efficiency, robustness, miniaturization, and communications capability. The past years have shown how far sensor technology can progress; photonics has definitely largely contributed to these advances. Photonic sensors, indeed, offer fast, light, cheap, and small-footprint components and products, very often characterized by high functionality and low energy usage. Further advances can be expected due to the development of quantum photonics: quantum control over light–matter interactions would enable new classes of measurement and communications solutions that have not been possible so far.

Recently, significant achievements have been made possible by devices pertaining to the class of resonant whispering-gallery-mode (WGM) microcavities [or whispering-gallery-mode resonators (WGMRs)]. Dielectric 2-D microresonators with circular or quasi-circular (e.g., slightly elliptical) planar symmetry, and the corresponding 3-D devices with spherical (spheroidal) or cylindrical symmetry, support confined propagation modes, which possess outstanding properties: these devices simultaneously hold unprecedented potential for a wide range of applications and constitute a great platform with which to explore fundamental physics.[1] Current technology allows us to fabricate, in many different materials, microresonators with a small modal volume V (and therefore a high energy density), very high quality factor Q, and large free-spectral range (FSR). The geometries range from microrings and microdisks to capillaries, microspheres, microbottles, and microbubbles. These microresonators have already demonstrated their excellent characteristics not only in the field of sensing, and biosensing, in particular, but also in the areas of lasers, nonlinear optics, and quantum information processing.[1–4] The following are a few recent examples of the miniaturization and device performance achievable with the WGMR technological platform:

1. Ultra-small (<2 μm in diameter) microring and microdisk lasers with an asymmetric air/GaAs/$Al_{0.98}Ga_{0.02}As$ waveguide and an active region based on InAs/InGaAs/GaAs quantum dots emitting around 1.3 μm.[5]
2. A thermodynamical-noise-limited microlaser at 1.56 μm using the dual WGM super-cavity approach (with 2-mm-sized MgF_2 cavities), exhibiting a fractional frequency instability of 1.7×10^{-13} at a 0.1-s integration time, corresponding to a fundamentally thermal-noise-limited integral linewidth of 8.7 Hz.[6]
3. By using a 3-mm silica spherical resonator (FSR ≈ 22 GHz) for experimental comparison, closed-form expressions for the Raman self-frequency shift and the efficiency of dissipative Kerr cavity solitons have been derived, which should be applicable to predict soliton behavior in any microcavity system.[7]

4. A hybrid silicon-core, silica-clad microspherical resonator (with a ∼115-μm outer diameter and ∼108-μm inner diameter) was proved to permit Kerr-based all-optical modulation of a weak probe on the timescale of femtosecond pump pulses.[8]
5. An experimentally feasible protocol for the implementation of quantum information transfer, using the effective dipole–dipole interaction between nitrogen vacancy (NV) centers coupled to a microresonator (e.g., NV centers in diamond nanocrystals coupled to a microsphere cavity). This scheme may represent a promising step toward the realization of quantum communications.[9]
6. A plasmon-enhanced WGM microcavity sensor consisting of a silica microsphere with a radius ranging from 30 to 50 μm, loaded with $\sim 12\,\text{nm} \times 12\,\text{nm} \times 42\,\text{nm}$ gold nanorods, exhibiting single-molecule sensitivity and selectivity to specific single binding events.[10]

With reference to this last application, it has to be underlined that WGMRs have permitted the implementation of some of the most sensitive optical sensing devices currently known.[1,11–15] The resonances of these microcavities can in fact be tuned by acting, on one side, on their shape, size, and material composition, and, on the other side, changing the boundary conditions (e.g., pressure or temperature). In turn, any change in the environment of a microresonator produces a variation in the frequency and/or the linewidth of the resonance, which can be measured with great accuracy.

Thus, advanced sensing applications of WGM microresonators are the main subject of this Spotlight, which first provides an outline of the basic characteristics and properties of these devices. Particular attention is paid to microresonators with spherical symmetry (spheres and bubbles) fabricated in glassy materials, which are the simplest to fabricate, while exhibiting ultra-high Q-factors. As an example, a Q-factor close to 10^{10} and a cavity finesse F larger than 10^6 were measured for a pure silica microsphere at a wavelength of 850 nm (this quality factor is close to the fundamental material absorption limit at that wavelength),[16] and an intrinsic Q-factor of 1.1×10^{10}, associated with a loss-limited finesse value of $\sim 4 \times 10^7$, was measured in a 90-μm-diameter microsphere made of 0.08 mol% erbium-doped ZBLALiP glass.[17] Referring to these devices, the issues of fabrication and of light coupling are also discussed. Finally, a number of examples of the sensing capabilities of the WGM microresonators are outlined.

2 Whispering Gallery Mode Resonators

The optical modes of dielectric spherical particles were studied for the first time by Mie in the early 19th century.[18] The spectrum of the scattered light shows very narrow peaks, corresponding to the resonant circulation of the light close to the surface of the spherical particle. These optical modes are confined at the air–dielectric interface by total internal reflection and are usually called

WGMs. Lord Rayleigh introduced the name when he explained the acoustic propagation phenomena caused by continuous reflections on the curved dome walls of St. Paul's Cathedral in London.[19] Other authors have called these modes morphology-dependent resonances;[20] this, however, is not a widespread term.

A quick and intuitive analysis of the propagation can be carried out simply by using geometrical optics. A ray of light undergoes total internal reflection if the angle of incidence Θ is larger than the critical angle $\Theta_c = \arcsin(\frac{1}{N})$. Figure 1 illustrates the phenomenon, where R is the radius of the sphere, and N_s is its refractive index. A dimensionless size parameter is generally introduced, defined as $x = 2\pi R/\lambda = kR$, where k is the wavenumber. For large spheres ($R \gg \lambda$ or $x \gg 1$) and rays at glancing incidence ($\Theta \sim \pi/2$), the propagation of the light is confined in the region between the sphere's surface and an internal spherical surface, whose tangents correspond to the critical angle at the sphere surface; the resonance condition requires that the optical path length, which should correspond to an integer number of wavelengths in order to remain in phase, is approximately equal to the circumference of the sphere:

$$2\pi NR = l\lambda, \tag{1}$$

where l is an integer.

The geometrical optics description has severe limitations: for example, it can neither explain how the light can couple into a WGM (or escape from a WGM) in a perfect sphere nor take into account the polarization of light. A complete description can be provided by the electromagnetic theory, and the resonances can be analyzed using the generalized Lorenz–Mie theory.[21] A detailed description of the mathematical theory can be found in various review papers.[1,4,12,13] The optical modes of dielectric spherical particles can be calculated by solving the Helmholtz equation in spherical coordinates. A comprehensive overview is provided by Oraevsky.[22] For an isotropic medium, the wave equation can be

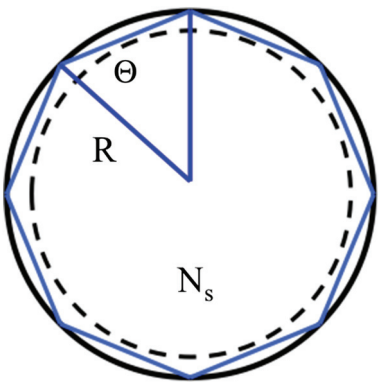

Figure 1 Total internal reflection of an optical wave in a caustic region of a microspherical resonator.

solved in its scalar form, with two solutions: the electric type, also known as transverse magnetic (TM) modes, and the magnetic type, or transverse electric (TE) modes. The Helmholtz equation can be solved using the separation-of-variables approach:

$$\Psi_{\ell,m,n}(r,\theta,\varphi) = \Psi_r(r)\Psi_\theta(\theta)\Psi_\varphi(\varphi). \tag{2}$$

The eigenfunctions that describe the radial, polar, and azimuthal components can be associated with the radial (n), polar (ℓ), and azimuthal (m) quantum numbers, as well as the polarization. The eigenfunctions are given by the following equation:

$$\frac{d^2\Psi_\ell(r)}{dr^2} + \left[N^2(r)k^2 - \frac{\ell(\ell+1)}{r^2}\right]\Psi_\ell(r) = 0. \tag{3}$$

It is very similar to the Schrödinger equation of a particle with a mass M in a pocket-like pseudopotential V_{eff}, depending on energy

$$\left[-\frac{\hbar^2}{2M}\Delta + V_{\text{eff}}(r)\right]\psi(r) = E\psi(r), \tag{4}$$

where $E = \frac{\hbar^2 k^2}{2M}$ and

$$V_{\text{eff}}(r) = \frac{\hbar^2}{2M}\left\{[1 - N^2(r)]k^2 + \frac{\ell(\ell+1)}{r^2}\right\}, \tag{5}$$

$$\frac{1}{\cos(\theta)}\frac{d}{d\theta}\left(\cos(\theta)\frac{d}{d\theta}\Psi_\theta\right) - \frac{m^2}{\cos^2(\theta)}\Psi_\theta + \ell(\ell+1)\Psi_\theta, \tag{6}$$

$$\Psi_\varphi = \frac{1}{\sqrt{2\pi}}\exp(\pm im\varphi). \tag{7}$$

Briefly, the radial component Ψ_r of the total electromagnetic field is described by a spherical Bessel function inside the microsphere ($r \leq R_0$), while externally ($r > R_0$) the field decays exponentially away from the microresonator surface. The polar contribution Ψ_θ is often expressed by spherical harmonics associated with Legendre polynomials, whereas the azimuthal dependence Ψ_φ is given by a linear combination of periodical functions $\sin(m\varphi)$ and $\cos(m\varphi)$. For each polar number ℓ, the allowed azimuthal mode numbers are in the range of $-\ell < m < \ell$, leading to a $2\ell + 1$ degeneracy of the azimuthal modes. Figure 2 shows a rendered image of a qualitative field distribution in the case of the fundamental WGM with $\ell - m = 2$. The presence of an evanescent field tail at the

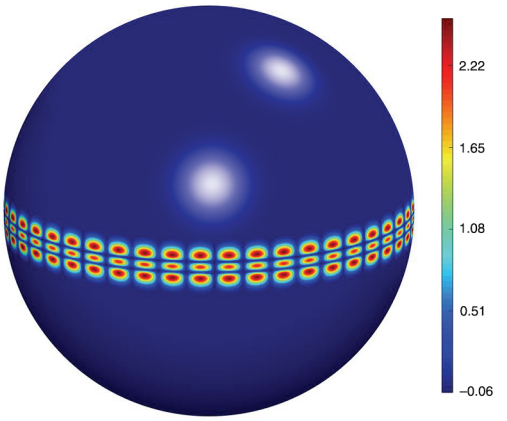

Figure 2 A 3-D rendered image of a qualitative field distribution in a fundamental WGM with $l - m = 2$.

microsphere boundary explains the possibility to excite the WGMs inside the spherical microresonator by means of suitable coupling systems. An analogous procedure can be applied for other geometries by simply changing the coordinate system.

The position of the resonances, in term of the size parameter, is then given by the following equation:

$$Nx_{\ell,n}^{P} \approx \ell + \frac{1}{2} + \left(\frac{\ell + 1/2}{2}\right)\left[\frac{3\pi}{2}(n - 1/4)\right]^{\frac{1}{3}} - \frac{P}{\sqrt{N^2 - 1}}, \tag{8}$$

where $P = N$ for TE modes, and $P = 1/N$ for TM modes. A number of characteristics of the WGM spectrum can be obtained from this equation, including the quasi-periodicity for WGMs with the same n value and $\Delta\ell = 1$ corresponding to a pseudo-FSR Δ_0 given by

$$\Delta_0 = \frac{2}{\pi NR}, \tag{9}$$

and the spacing between modes having the same quantum numbers but different polarizations Δ_P is given by

$$\Delta_P = \Delta_0 \sqrt{\frac{N^2 - 1}{N^2}}. \tag{10}$$

The modes with the smallest mode volume, which are of greater interest in many applications, are those with low n values and with $m \approx \ell$, and they are most closely confined to the surface of the sphere. In this case, the propagation constant β for the WGMs can be written simply as

$$\beta = \frac{k\ell}{x_{n,\ell}}. \tag{11}$$

More-detailed descriptions of the mathematical solutions can also be found in some of the references.[1,4,23]

2.1 Quality factor of a whispering gallery mode

The key parameter of microspherical resonators in many applications is their quality factor Q. It can be considered as an indication of the fraction of light lost during each cycle around the sphere. The intrinsic Q of a microsphere is determined by contributions coming from several types of losses

$$Q^{-1} = Q_{\text{rad}}^{-1} + Q_{\text{scat}}^{-1} + Q_{\text{mat}}^{-1} + Q_{\text{cont}}^{-1}, \tag{12}$$

where Q_{rad} denotes intrinsic curvature losses, Q_{scat} denotes scattering losses on residual surface inhomogeneities, Q_{mat} denotes intrinsic material losses, and finally Q_{cont} indicates the losses introduced by surface contaminants. This separation is valid only for weak losses. Q_{rad} vanishes exponentially with increasing size, so with $2R/\lambda \geq 15$, $Q_{\text{rad}} > 10^{11}$. Calculations based on the model of Rayleigh scattering by molecular-sized surface clusters under grazing incidence and total internal reflection yield the following estimate for Q_{scat}:

$$Q_{\text{scat}} \approx \frac{3\lambda^2 \ell^{10/3}}{16\pi^5 \sigma^2 N^2 n^{5/2}}. \tag{13}$$

Introducing the correlation length of the inhomogeneities B and the diameter D of the sphere, Gorodetsky et al.[24] produced a new equation in 1996:

$$Q_{\text{scat}} = \frac{\lambda^2 D}{2\pi^2 \sigma^2 B}. \tag{14}$$

Fused silica resonators present scattering parameters $\sigma \leq 3$ nm and $B \simeq 5$ nm, but in this case, the diffusion of atmospheric water into the material fixes the upper limit for the intrinsic Q-factor to Q_{cont}. For a millimeter-sized resonator, Maleki et al.[25] have fabricated, by polishing techniques, crystalline optical resonators with a very high Q-factor ($Q > 10^{11}$) limited in value only by the absorption of the material (Q_{mat}) and exceeding that of surface-tension-formed resonators. The main limit of the WGM Q-factor is indeed related to the contribution Q_{mat} associated with the absorption and bulk Rayleigh scattering in the material constituting the microresonator. Considering an attenuation β in dB/km, Q_{mat} can be approximated by

$$Q_{\text{mat}} \approx \frac{4.3 \times 10^3}{\beta} \frac{2\pi N}{\lambda}. \tag{15}$$

Because the optical attenuation of undoped silica glass is around $\beta \sim 0.2$ dB/km at $\lambda = 1.55$ μm, Q_{mat} may reach a value of $\approx 10^{11}$. The experimental Q-factor of silica microspheres is much lower (between a few 10^8 and 10^9)[24,26] because one has to take into account the contribution Q_{cont}, which denotes the losses introduced by surface contaminants during the fabrication process. Gorodetsky et al.[24] attributed most of this reduction to the absorption of radiation by a nanolayer of molecules (first of all, water molecules) adsorbed on the microsphere surface.

Due to a high Q-factor, resonances can also occur in doublets because the very low scattering allows one to split the WGMs in clockwise (defined by n, ℓ, m numbers) and counter-clockwise (defined by n, ℓ, $-m$ numbers) propagation.[27]

The Q-factor can be determined either by the measurement of the cavity-ringdown decay time ($Q = 2\pi\nu\tau$) or, if the spectral purity of the laser probe is adequate, by the conventional measurement of the transmission bandwidth:

$$Q = 2\pi\nu\tau = \frac{\delta\lambda}{\lambda}. \tag{16}$$

Finally, another characteristic parameter of a resonator is its finesse F. The Q factor of an optical resonator equals the finesse F times the optical frequency divided by the FSR. Usually, F and Q are equally important in the applications; in some cases, however, finesse is more useful than the quality factor. The buildup of optical power inside the resonator, for instance, is proportional to the finesse.

The efficient coupling of light in or out of a microsphere is a key issue and requires the use of near-field coupling: the evanescent field of a phase-matched optical waveguide should overlap with the evanescent field of a WGM. Figure 3 shows that when the gap between the coupler and the resonator is too large, there is no propagating wave inside the resonator because the evanescent wave of the coupler decays exponentially over a short distance from the boundary. On the contrary, when the coupler and resonator are close enough, light can be easily coupled into the resonator by optical tunneling.

Selective excitation of high-Q WGMs (lowest n values) is possible through the use of phase-matched wave coupling from an adjacent waveguide or a prism under frustrated total internal reflection. Different couplers, such as a prism, eroded fiber coupler, tapered fiber, angle-polished fiber coupler, and strip-line waveguide, have been experimentally demonstrated. Detailed descriptions of the different coupling systems can be found in a very recent paper by the authors[14] and, for the pros and cons, readers are referred to previous papers.[1,4,28]

Coupling can be characterized by the fractional depth K of the resonance dip in the intensity transmittance through the coupler.[29] K is observed while

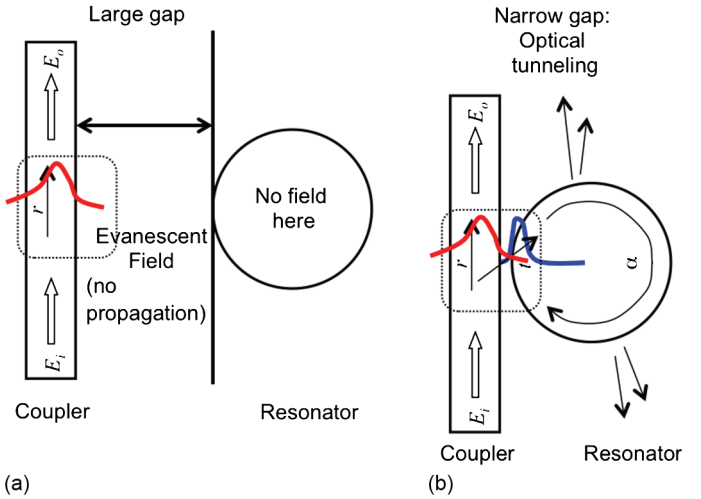

Figure 3 Coupling conditions: (a) light cannot be coupled into the resonator since the gap is too large and (b) when the gap is narrow, optical tunneling can occur and the light can be coupled into the resonator.

varying the frequency of the exciting wave around the resonance and can be expressed in the following way as a function of the intrinsic quality factor of the WGM Q_0:

$$K = 4\frac{Q_0 Q_c \Gamma^2}{Q_0^2 + Q_c^2}, \tag{17}$$

where Q_c describes loading, i.e., it is proportional to the inverse of the transmittance of the coupler, and the coefficient Γ describes the mode-matching (a single-mode coupler is always mode-matched). The quality factor of the system Q_s is related to Q_0 and Q_c by the following equation:

$$Q_s^{-1} = Q_0^{-1} + Q_c^{-1}. \tag{18}$$

Unlike the case of Fabry–Perot cavities with their fixed coupling to external beams, the sphere-coupler system provides a unique opportunity to easily control the bandwidth of the cavity. In fact, Q_s can be adjusted by increasing the gap between the coupler and the sphere from the over-coupled regime ($Q_c \ll Q_0$) to the under-coupled one, which permits a clear observation of saturation of the measured Q_s up to its intrinsic (unloaded) value Q_0 (Fig. 4). Maximum contrast is achieved when the coupling losses equal the intrinsic cavity losses, i.e., $Q_c = Q_0$ or $Q_s = \frac{1}{2}Q_0$, and the entire coupled power is lost inside the resonator (Fig. 5). This regime is usually referred to as critical coupling.

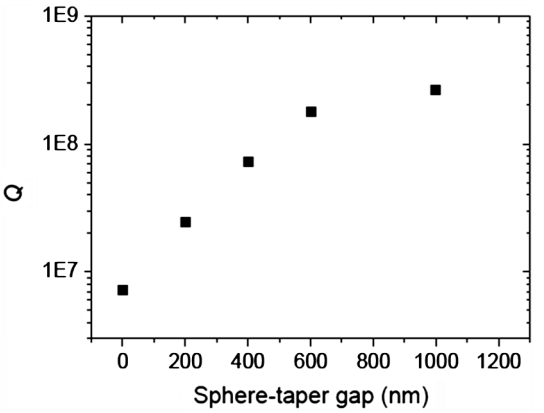

Figure 4 Measured Q values versus fiber-microsphere gap. The Q factor saturates to its intrinsic value $Q \sim 3 \times 10^8$. Reproduced from Ref. 29.

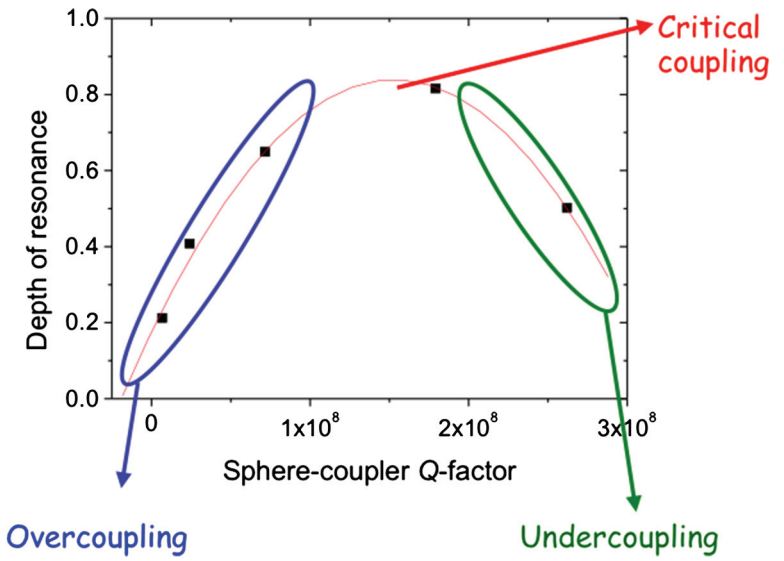

Figure 5 Depth of resonance K versus sphere-coupler system Q factor.

In most cases, Q values are obtained by measuring the resonance linewidth of the WGM modes using a tunable external-cavity laser with a linewidth of a few hundreds of kHz as the light source; a typical laboratory setup is sketched in Fig. 6. The laser can be finely swept at very low frequency (100 Hz) around a resonance by a few GHz. The experimental setup for the microresonator's characterization can be realized with standard fiber-optic components, either spliced or connected with APC connectors. The out-coupled light is monitored at the output of the taper using a photodiode detector connected to an oscilloscope. The

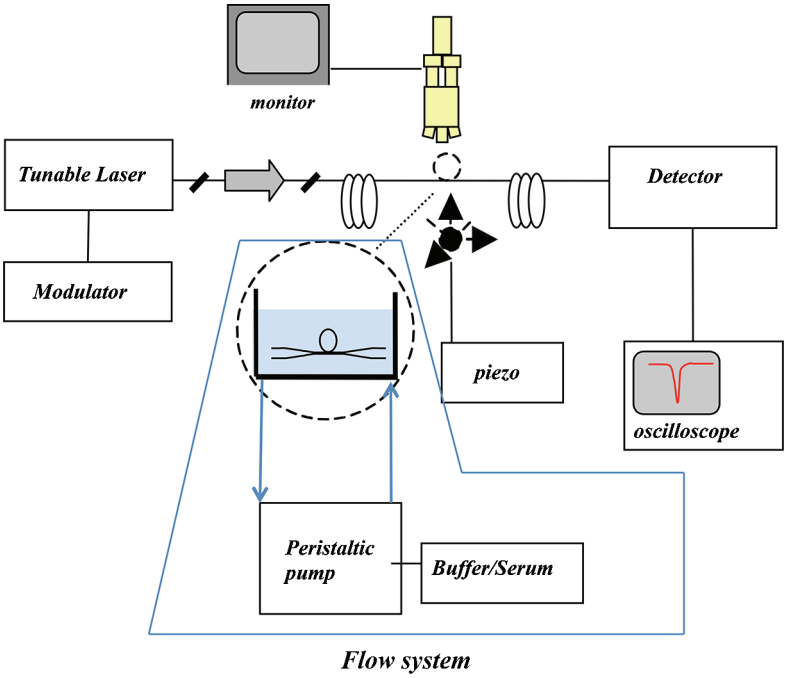

Figure 6 Sketch of a typical experimental setup for measuring the *Q* values, even inside a flowing liquid.

coupling efficiency from the fiber taper to the microsphere (in-coupling) can be gradually increased by reducing the gap between the sphere and the taper, thus affecting both the resonance width and depth; by using two microscopes, the alignment may be controlled in both the horizontal and the vertical planes. As an example of the necessary laboratory equipment, the following is a list of the instruments and components used for Q measurements around 1550 nm:

– tunable laser diode (Yenista, Tunics),
– modulator (Agilent, 33250A),
– optical fiber (Corning, SMF-28),
– microscopes (Navitar, Zoom 6000, modular kit),
– *x*-*y*-*z* piezoactuators (PI-Instruments, Nanocube),
– detector (InGaAs),
– oscilloscope (Tektronix, DPO7104),
– peristaltic pump (Gilson, Minipuls 3) or syringe pump (KD Scientific, KDS220), and
– CCD camera and monitor (any will fit).

In a real sensing operation, the over-coupled regime is preferred because it helps to improve the resilience to ambient fluctuations, liquid flow, and geometrical changes. In a sensing experiment, for instance, one has also to take into

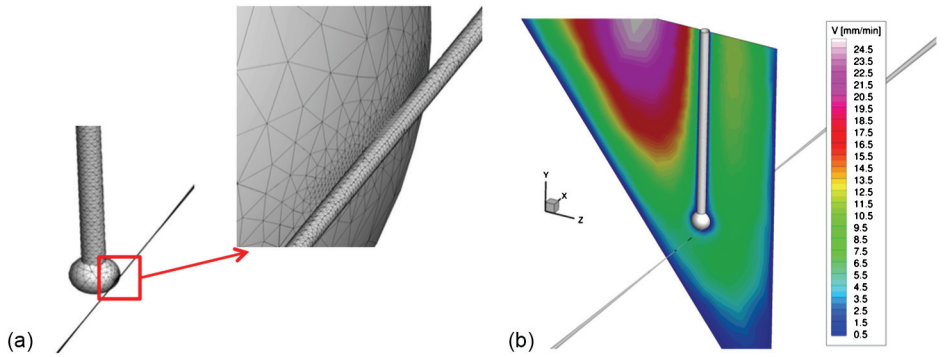

Figure 7 (a) Microsphere in contact with a tapered fiber in an over-coupled regime. (b) Transverse profile of a fluidic cell with the calculated flow velocity distribution. The flow is not uniform; it is higher at the upper surface (free) of the cell.[30]

account that the velocity magnitude of the flow in an open cell is higher near the free surface; thus, when the analyte is injected in the solution, the time required to reach the sensor depends on the injection zone. Figure 7(a) shows a microsphere and a tapered fiber in contact in a sensing experiment; Fig. 6(b) shows the transverse profile of a fluidic cell with the calculated flow-velocity distribution.[30]

3 Different Types of Whispering Gallery Mode Resonators

WGMRs can be classified according to their geometry, e.g., spheres, toroids, bottles, bubbles, disks, rings, cylinders, and capillaries. These devices can be fabricated using various materials, such as glass, quartz, silicon (as well as other semiconductors), silicon-on-insulator (SoI), silicon nitride, polymers, and crystals. All of these devices are highly suitable for sensing applications because they share excellent properties, namely, a high Q factor, tunability, and high stability and sensitivity; moreover, only a small sample volume is needed to detect a given analyte. Sensing by a WGMR can be considered a miniaturized and updated version of the conventional optical cavity ring-down spectroscopy,[31,32] where long and bulky conventional Fabry–Perot resonators are used to obtain an effective optical path-length sufficient to enable a high resolution. Figure 8 shows optical and SEM images of the microresonators described in the following subsections.

3.1 Microring and microdisk resonators

Microring and microdisk resonators have lower Q factors than other WGMRs, but they have the advantage of being easily fabricated in planar arrays using lithographic or imprinting technologies, together with adjacent single-mode port waveguides for in- and out-coupling the light to and from the resonator; the port waveguides can be arranged horizontally or vertically. Integrated WGMRs have

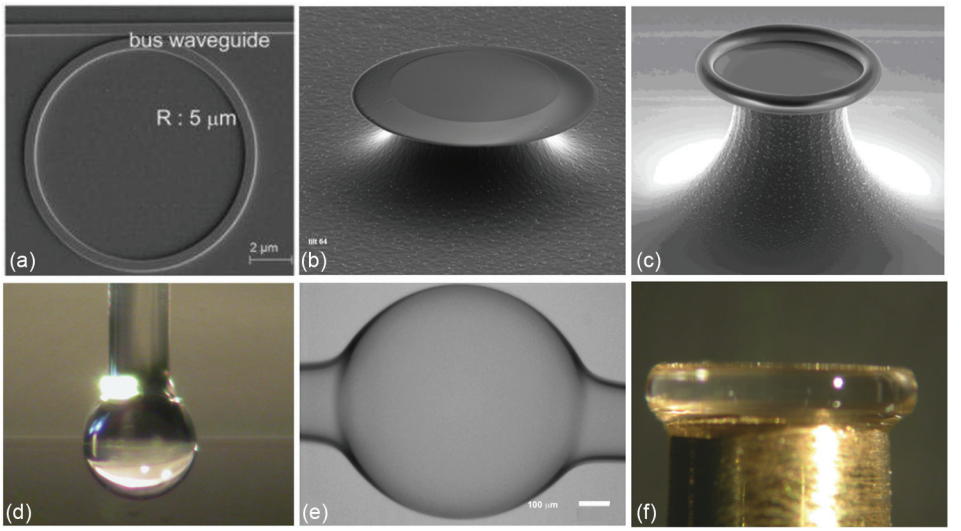

Figure 8 (a) SEM image of a microring resonator with a radius of 5 μm and the bus waveguide that acts as a coupler. (Reproduced with permission from Ref. 33—Copyright 2010 American Chemical Society.) (b) SEM image of a microdisk resonator. (Reproduced with permission from Wikimedia—Itay Shomroni.) (c) SEM image of a microtoroid. (Reproduced with permission from Ref. 34). (d) Optical image of a microsphere with $d \sim 150\,\mu m$. (e) Optical image of a microbubble. (f) Optical image of a millimeter-sized LN crystalline disk.

been fabricated using a variety of materials—namely, silicon oxide,[35] silicon nitride,[36] SoI,[37] polymers,[38,39] porous silicon[40]—and also in different shapes, such as rings, disks, racetrack rings,[41] goblets,[42] wedge disks,[43] and grating ring resonators.[44] New structures, such as the PANDA ring resonator, have also been designed, especially to exploit the nonlinear optical properties of the material.[45] The PANDA structure consists of a center ring with a radius of a few micrometers and two nonlinear side rings with a radius of 1 to 2 μm; the suggested material is InGaAsP/InP, which is nonlinear.

Recently, Q factors up to 10^7 have been demonstrated with extremely low-loss waveguides in Si_3N_4[46] and in SoI;[47] exceptionally small-footprint devices, with disks of a few microns in diameter, have been fabricated as well. Their use as a platform on a Si chip for quantitative and qualitative biosensing applications was successfully explored.[48] A very important feature of planar integrated WGMRs is the high multiplexing capability, which is very limited in other resonators, such as microspheres and microtoroids.

Millimeter-sized disks made in high-purity crystals exhibit a very high Q due to the very low intrinsic absorption of light within their transparency window.[49] Enhanced nonlinear or electro-optical properties may play an additional role for the implementation of high performance devices. This is the case of resonators made of lithium niobate (LN) that can be used for a number of devices, including

single- and multi-order tunable filters, electro-optic modulators, and frequency converters.[50] As an example, LN disks 4.7 mm in diameter were made from commercial 3 × 1 mm^2-thick Z-cut LN wafers by core drilling a cylinder and thereafter polishing the edge into a spheroidal shape.[51] Recently, femtosecond laser micromachining of LN films, followed by focused ion beam (FIB) milling, has been used to produce LN microdisks with a diameter around 80 μm and a Q up to 2.5×10^5.[52] Even better results were achieved when fabricating LN microdisk resonators on a LN film on an insulator wafer, which has a layer of silica lying between a thin LN film and a thick LN substrate, using only conventional semiconductor fabrication processes. The quality factor of a LN resonator with a 39.6-μm radius and a 0.5-μm thickness was measured to be around 1.19×10^6.[53]

3.2 Microtoroid resonators

Armani et al.[54] were the first to fabricate ultra-high Q toroidal microcavities. The material used was an oxide-coated Si wafer, and the fabrication process included photolithography, wet and dry etching, and laser reflowing. The laser reflowing was used to create a very smooth surface, as it effectively removes lithographic flaws, and also to fabricate an optical isolated toroidal structure as the disk shrinks. Very recently, an effective method was developed to fabricate ultra-high Q microtoroids with a picometer-precise resonant wavelength;[55] this method adds a second tuning reflow process, using low-power CO_2 laser pulses, to the traditional fabrication process. It is possible to control the shift of a WG mode with picometer accuracy by choosing an appropriate tuning reflow power, which is <25% of the power used for fabrication reflow. Meanwhile, the quality factor remains nearly unchanged during the tailoring process.

Compared to other WGMRs, microtoroids can be fabricated in planar arrays, but the coupling system is still external to the array, reducing the multiplexing capabilities. Microtoroid optical resonators have been used in a biological and chemical sensing system known as a frequency-locked optical whispering evanescent resonator that combines frequency-locking feedback control, balanced detection, and data-processing techniques to achieve single-macromolecule detection in an aqueous solution without the use of labels.[56]

3.3 Microsphere resonators

Microspherical WGMRs are extremely simple to fabricate, can reach extremely high Q factors, and were also the first WGMR tested as a biosensor. Microsphere resonators are usually fabricated by simply melting the tip of an optical fiber either with a hydrogen torch,[57] a CO_2 laser,[58] or a fiber splicer.[59] In all cases, the glass is heated and softened so that the surface tension forms a spherical object with very low surface roughness at the end of the fiber stem. If one starts from a conventional telecom fiber, with a cladding diameter of 125 μm, spheres

with diameters in the range of 125 to 350 μm can be easily produced. In order to obtain smaller spheres, the fiber needs to be tapered first; the taper is obtained by heating and stretching the fiber itself until it breaks. By melting the tip of the tapered fiber, spheres with a diameter down to about 25 μm can be obtained.[60] The fiber stem allows an easy positioning and alignment of the microsphere with respect to the coupling system. One of the main drawbacks of the coupling system is that the relative position of the microsphere to the signal fiber must be rigorously maintained during the measurements; otherwise, the detection of the resonance is compromised.

Another class of (almost) spherical WGMRs is that of droplet resonators: after the seminal papers by Chang and Campillo,[61,62] these liquid resonators are again gaining attention in the biosensing field.[23,63] Droplets are simultaneously a transducer and sample to be analyzed; in this case, the analytes incorporated into the droplet can interact with the stronger portion of the WGM rather than with the relatively weak evanescent tail, and this leads to a higher detection sensitivity.

3.4 Microcapillary resonators

Microcapillary resonators are also known as liquid core optical ring resonators (LCORRs) and are particularly suitable for liquid sensing.[64] Hollow-core glass capillaries confine light along their perimeter; they easily combine photonics with microfluidics in such a way that the optical layer is physically separated from the sensing layer. The concept of the LCORR, the theoretical analysis, and some experimental results related to the LCORR sensor development have been described in a review paper.[65] The sensitivity of LCORRs depends on the structural parameters of the capillary, i.e., radius and wall thickness; typical values of the capillaries used for biosensing are between 100 and 150 μm in diameter, with a wall thickness of around 3 μm. Sensitivity is improved by reducing the wall thickness because it enhances the overlapping of the WGMs fields with the analyte. It is, therefore, important to fabricate capillaries with thin walls, finding a good compromise in order to avoid fragility of the device.[66] Zamora et al.,[67,68] for example, developed a technique to fabricate microcapillaries with submicrometric wall and reported improved refractive index sensing capability. Quantitative real-time label-free detection of DNA sequences using a LCORR sensor was demonstrated as well.[69]

3.5 Microbottle and microbubble resonators

Sumetsky et al. pioneered two very interesting and promising cavity geometries: the microbottle[70] and the microbubble.[71] A microbottle resonator, or whispering gallery bottle (WGB) as named by Sumetsky, is obtained by deforming a cylinder (or tube) along its long axis so that the radius increases smoothly up to a maximum and then decreases again. WGBs combine standard WGMs with "bouncing

ball" modes, localized near the stable closed rays that experience multiple reflections from the cavity wall. WGBs, which routinely achieve Q-factors on the order of 10^7, in their simplest form, can be created from an optical fiber by use of the CO_2 laser heating technique in order to taper the fiber with a predetermined shape. An advantage of bottles with respect to conventional fiber-based microspheres is that the two stems allow one to tune the WGB microcavity simply by stretching the fiber. WGBs can be either solid or hollow.[72]

Among the hollow resonator structures, however, microbubbles are the most interesting for sensing applications. Sumetsky fabricated the first microbubbles by rotating a pressurized capillary heated by a CO_2 laser beam; by controlling the gas pressure and the laser power, the size of the bubble and the wall thickness can be optimized.[71] Berneschi et al.[73] used a different method of fabrication, which allowed them to reproducibly obtain high-Q microbubbles. In this case, the static pressurized capillary was heated by the arc discharge created by two rotating electrodes.[73] Given the importance of a very thin bubble wall (no more than 3–4 μm for an efficient interaction between the WGM and the inner flow), a nondestructive method was developed to measure the wall thickness.[74]

Very recently, the fabrication of ultra-thin walled (approaching 500 nm) silica microbubbles with Q-factors of about 10^7 at the telecommunications C-band has been reported.[75] The authors, by introducing two figures-of-merit (FoMs), i.e., $\mathrm{FoM}_1 = Q \times 10^{\lambda/t}$ for the wall thickness and $\mathrm{FoM}_2 = Q \times 10^{\lambda/R}$ for the radius, have also compared microbubble resonators produced by different fabrication methods.

Microbubbles, like LCORR, separate the fluid layer from the optical layer, warranting no alignment disruption between the bubble and the coupling system due to interaction with the analyte flow.

Table 1 summarizes the fabrication methods of the various microresonators, as described in greater detail in previous subsections; here, they are listed in alphabetical order. This list is definitely not exhaustive, but it provides a good overview of the most common resonator structure/material/fabrication technique combinations.

4 Sensing Principles

For the sake of simplicity, this section refers to microspherical resonators: the frequency (or wavelength) locations of the peaks in the resonance spectrum depend on the size, shape, and refractive index of the microsphere. A frequency shift of the resonance(s), when the radius and/or the refractive index of the sphere changes, makes possible the utilization of this WGMR for the detection of trace amounts of chemicals and biological molecules or of minimal physical changes in the environment. This phenomenon is called a reactive mechanism: the interaction of the particles with the WGMR is resonantly reinforced. When a particle aggregates at the surface of the resonator, it interacts with the evanescent part of

Table 1 Fabrication techniques of WGMRs.

Type and material	Fabrication method	Ref.
Droplet, suspended	Spraying; syringe or glass wire	76
Droplet, hemispherical	Hydrophobic spreading or self-assembly	77 and 78
Microbottle	Heat and pull or soften and compress an optical fiber	72
Microbubble	Heat a pressurized optical fiber	73 and 79
Microcapillary (LCORR)	Glass tube drawing and etching	65 and 67
Microdisk, LN	Photolithography + etching	53
Microdisk, LN	Femtosecond-laser machining + focused ion beam	52
Millimeter-disk, crystalline LN	Optical polishing	51
Microdisk, silicon	Nanoimprinting	80
Microdisk, Si-rich nitride	Photolithography + etching + annealing	81
Micropillar	*In situ* optical or e-beam lithography	82
Micropost, semiconductor	E-beam lithography + etching	83
Microring	Optical or e-beam lithography	84
Microsphere, glass	Glass melting and pouring or plasma torch	85–87
Microsphere, glass	Sol-gel process	88
Microsphere, PDMS	Electrohydrodynamic lithography	89
Microsphere, π-conjugated polymer	Vapor diffusion self assembly	90
Microsphere, silica	Silica fiber tips melting	4
Microtoroidal resonator, silica	Optical lithography + etching + laser reflow	55 and 91
Microtoroidal resonator, silicon	Optical lithography + H_2 annealing + wafer bonding	92
Microtorus	Mechanical compression of a silica glass sphere	93
Racetrack resonator	E-beam lithography + RIE	94
Racetrack resonator, polymer	Optical lithography + RIE or photodefinition	95

the WGM field, inducing not only a shift in the wavelength but also a change in the Q factor. In fact, the interaction of the WGMR with the external particles usually introduces additional losses, thus inducing a line broadening and therefore, a change of the quality factor. Measuring the line broadening is currently a complementary sensing mechanism to the measurement of the reactive shift.[13,23] In a high-Q WGMR, mode splitting can also be used as a detection system.[27]

4.1 Reactive shift

The resonant wavelength changes can be written as follows:

$$\frac{\Delta\lambda}{\lambda_0} = \frac{\Delta R_0}{R_0} + \frac{\Delta N_s}{N_s}, \tag{19}$$

which states that any small change in the refractive index and/or in the radius must be balanced by a small change in the resonant wavelength. This approach is not valid for complex molecules, such as proteins.[96–98] Biological molecules binding to the WGMR surface, in fact, shift the resonance due to their excess of polarizability α_{ex} that is proportional to the molecular weight

$$\frac{\Delta\lambda}{\lambda} = \alpha_{ex}\frac{\sigma}{\epsilon_0(N_s^2 - N_m^2)R_0}, \tag{20}$$

where σ is the surface density of molecules forming a layer, and N_s and N_m are the refractive indices of the sphere and the medium, respectively. Equation (20) describes only the shift but not the limit-of-detection (LoD). More detailed discussions about first-order perturbation theory for obtaining the shift can be found in the literature.[99,100] One can assume that the field of a particular molecule is not influenced by its neighbors[98] and take into account that the lowest surface density that can be detected depends on the resonance linewidth $\delta\lambda$ (or a fraction F of the linewidth), which in turn depends on the quality factor $Q = \delta\lambda/\lambda$.[11] Accordingly, the LoD of the surface density may be given by[11,21]

$$\sigma_{LoD} = \frac{\epsilon_0(N_s^2 - N_m^2)R_0F}{\alpha_{ex}Q}. \tag{21}$$

Some years ago, a paper was published providing a theory for comparing reactive and thermo-optical mechanisms.[101] The thermo-optical mechanism is due to the heating of the protein layer through linear absorption and its transfer to the WGMR. This local heating is proportional to the imaginary part of the polarizability and causes an additional shift of the resonant frequency. The authors concluded that such a thermal effect is several orders of magnitude smaller than the reactive mechanism and therefore cannot be used as an enhancement mechanism in label-free biosensing. On the contrary, the thermo-optical mechanism is usually a limitation in a WGMR-based sensor.[102] Le et al. investigated a novel method

based on the differential frequency of TE and TM modes to reduce the thermal noise baseline. The method eliminates the effect of thermal expansion and thermoelasticity on the resonance peaks. The authors estimated an LoD of 10^{-8} refractive index units (RIUs), assuming a temperature-controlled environment with $\Delta T \sim 0.01°C$.[102]

The possibility of enhancing the detection of nanobioparticles in a solution has been explained by Arnold et al.,[103] who reported the observation and analysis of an optical mechanism, named WGM Carousel, which increases the transport rate of nanoparticles (NPs) to the sensing volume of a microspherical silica resonator by more than 50 times. The Carousel is an optical trap mostly due to the evanescent optical gradient forces generated with only microwatts of driving power. By controlling the ionic strength of the buffer solution and the optical trapping power, particles are shown to bind preferentially within the Carousel.

4.2 Mode splitting and line broadening

Ultra-high Q resonators possess degenerate WGMs, with the same resonant frequency and field distribution but propagating in two different directions, clockwise and counter-clockwise. The degeneracy could be split into two modes due to surface roughness, material inhomogeneity, or the addition of a surface scatterer. Yang et al. explained in an intuitive way the split phenomenon when a scatterer is close to the WGMR surface: the scatterer acts as a damping channel, from which a part of the scattered field is lost to the environment, while the rest of the field is coupled back into the WGMR, inducing the mode splitting.[27] In this case, the linewidth broadening Γ_S is given by the difference between the linewidths of the split modes (see Fig. 9) that can be calculated using the dipole scatterer approach as $\alpha\omega^4 f^2(r)/(6\pi c^3 V)$, where α is the polarizability of the scatterer, ω is the resonance frequency, V is the mode volume, c is the speed of the light, and $f(r)$ is the normalized mode distribution at the position r. The detection limit in this case can be estimated from the expression:

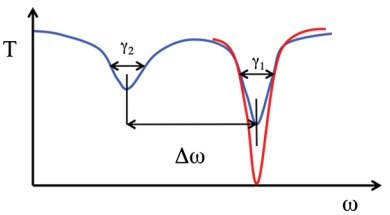

Figure 9 Sketch of the transmitted line shape before (red) and after (blue) mode splitting induced by a scatterer. $\Delta\omega$ is the detuning between the symmetric and asymmetric mode, γ_1 and γ_2 are the linewidths of the split modes. The scatterer is detectable when $\Delta\omega > (\gamma_1 + \gamma_2)/2$.

$$\alpha\omega f^2(r)/V > \Gamma_S + \omega/Q => 2|g| > \Gamma_S + \omega/Q. \tag{22}$$

In order to increase the feasibility and accuracy of the mode-splitting measurement, an interferometric setup has been developed that allows the splitting to be quantified in real time with a bandwidth beyond 10 MHz even in a liquid environment.[104] In this way, the capacity is achieved to sense small, single unlabeled molecules: it may be an enabling technology to investigate single-molecular processes and protein folding.

Monitoring the line broadening is a quite new sensing mechanism,[105] which suffers less from the noise caused by the laser frequency and environmental temperature changes. When a particle is bound to the WGMR surface, additional losses due to absorption and scattering are introduced. Figure 10 sketches the frequency shift and line broadening, namely, the physical principle of the mechanism. The linewidth Γ of the modes can be obtained using a Lorentz fitting. In this case, the detection limit depends on the uncertainty σ of the measured linewidth, and it can be written as

$$\Gamma/2\pi > \sigma, \tag{23}$$

$$\Gamma = (1/2\pi)(\alpha\omega/V)[1 + \alpha\omega(6\pi c^3)]f^2(r), \tag{24}$$

where $\Gamma/2\pi$ is the resonance linewidth broadening of the cavity mode, and when caused by a Rayleigh scatterer, it can be described by Eq. (24), or, equivalently, by $2|g| + \Gamma_S$.

A theoretical analysis of detection limits in swept-frequency WGM biosensing techniques was developed, also presenting a quantification and comparison of detection sensitivity for both resonance shift and broadening sensing modalities.[106] In order to effectively compare the relative performance of the two sensing modalities, however, one has to take into account the properties of the particle to be detected. According to Foreman et al.,[106] for nonabsorbing particles,

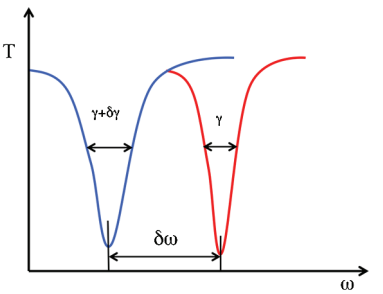

Figure 10 Sketch of the transmitted lineshape before (red) and after (blue) mode shift and line broadening. $\delta\omega$ is the frequency shift, γ is the initial linewidth, and $\gamma + \delta\gamma$ is the broadened linewidth of the shifted mode.

the performance of both modalities is comparable for smaller resonators, while broadening-based sensing surpasses the reactive-shift-based sensing for larger microcavities and when absorption in the particle is strong.

5 Whispering Gallery Mode Resonator Sensors: Applications

5.1 Sensing of physical parameters

The sensitivity of WGMRs to external changes can be exploited in sensors of physical parameters, such as temperature, pressure, force, and mass. Table 2 presents some applications of WGM microresonators in this area; the specific measurements are discussed in the subsections below.

In the case of temperature, the sensitivity of WGMR sensors can be extremely high. One of the first papers published by our group[59] was, indeed, about a temperature sensor; we were able to detect changes in the resonance wavelength of 14.2 ± 0.4 pm/°C around 27 °C and 16.4 ± 0.8 pm/°C around 54 °C. The sphere and the taper were placed inside an aluminum cell whose temperature was controlled by using Peltier pumps. The temperature inside the cell was monitored through a small-size glass sealed thermistor, which was placed in close proximity to the silica WGMR. The theoretical value of the temperature-dependent shift can be calculated as follows. The resonance wavelength λ is determined by the stationary condition, expressed by $\ell\lambda = \pi N d$, where ℓ is an integer, which defines the order of the longitudinal mode, and N and d are the refractive index and the diameter of the sphere, respectively. An increase of cavity temperature ΔT results in a sphere diameter increase Δd and in a change of index of refraction ΔN. Both changes affect the resonance, and the stationary condition can be rewritten as follows:

Table 2 Sensing of physical parameters by WGMRs.

Physical quantity	WGMR type and material	LoD	Ref.
Temperature	Microsphere, silica	14.2 pm/°C	59
	Microsphere, PDMS	0.245 nm/K	107
	Toroid, PDMS coated	0.152 nm/K	108
	Toroid, silk fibroin	−1.17 nm/k	109
	Microbubble, packaged	1.1×10^{-3} °C	110
Pressure, force, mass	Microsphere, silica	0.031 nm/N	111
	Microsphere, hollow, PMMA	7.664 nm/N	112
	Microbubble, silica	7 GHz/bar	113
	Toroid, silica	Sub-pg	114
Viscosity	Microbubble, silica	2.2 cP	115

$$\ell\lambda = \pi N d\left(1 + \frac{1}{N}\frac{\partial N}{\partial T}\Delta T\right)\left(1 + \frac{1}{d}\frac{\partial d}{\partial T}\Delta T\right). \tag{25}$$

By using the available data for the Corning SMF-28$^{(R)}$ silica fiber thermal expansion and thermo-optic coefficients at room temperature ($5.6 \times 10^{-7}\,°C^{-1}$ and $1.2 \times 10^{-7}\,°C^{-1}$, respectively), the calculated value of $\Delta\lambda$ is 13.5 pm/°C (at room temperature), which agrees with the measured value of 14.2 ± 0.4 pm/°C around 27°C (see Fig. 11). It can be noted that the index change with temperature accounts for the main part of the resonance shift.

Polymeric materials, when used for coating a silica WGMR or for the direct fabrication of a WGMR, represent an interesting solution to achieve thermal sensing and stabilization. Polydimethylsiloxane (PDMS) is a good choice, as proved by the work of Dong et al.,[107] who demonstrated sub-millikelvin temperature sensitivity with a tuning coefficient of 0.245 nm/K. A similar procedure was followed by Li et al.,[108] but they just exploited a PDMS coating onto a silica microtoroid to achieve an even lower tuning coefficient of 0.152 nm/K. Very recently, Xu et al.[109] demonstrated that silk fibroin toroids show a sensitivity eight times higher than the previous thermal sensors based on WGMR, due to the large thermal expansion coefficient of silk.

In another very recent paper, a packaged microsphere-taper system has been proposed for robust thermal sensing applications.[116] The WGMR was fixed to the fiber by UV optical glue and showed a temperature resolution of 1.1×10^{-3} °C. The package, besides being a thermal insulation, provides also mechanical stability.[110,116] A quite opposite approach has been followed by Petermann et al.,[117] who used an array of free PMMA microspheres, randomly placed on a microscope slide or on a fused-silica prism. This device, undoubtedly inexpensive and easy to manufacture, proved to be well suited for the

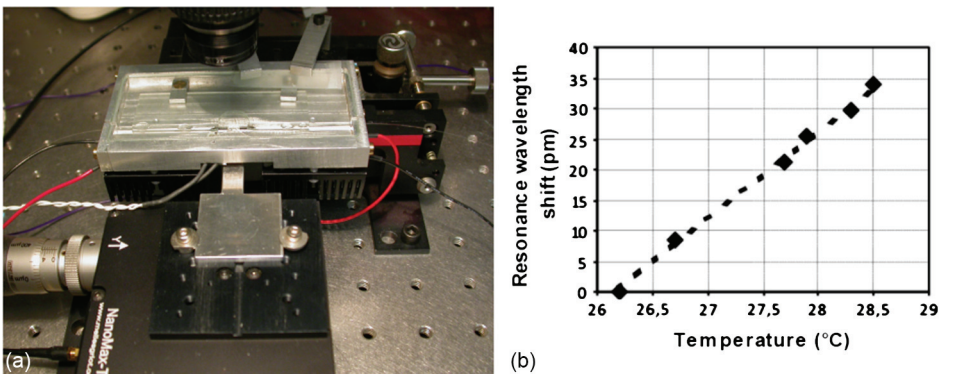

Figure 11 (a) Photograph of the thermostatic cell, where the microsphere sensor is placed. (b) Resonance wavelength shift versus temperature for a microsphere with a 350-μm diameter.

determination of an unknown wavelength or for temperature measurements, provided that a suitable calibration is available. As an example, an array of 18 commercial PMMA spheres with a mean diameter of 74.44 μm was used to realize a wavelength and temperature sensor with an accuracy of $\Delta\lambda = 0.01$ nm and a sensitivity of 0.001 nm/K, respectively.[117] Compressive forces and mechanical strains applied to a sphere may induce changes both in the shape and in the index of refraction of the sphere, again leading to a shift of WGMs. For solid silica microspheres of diameter about 430 μm, a sensitivity of about $d\lambda/dF = 0.031\,\text{nm/N}$ was demonstrated.[112] Fluorescent microspheres were used to measure biomechanical stress in a live cell during endocytosis.[118]

Hollow-core WGMRs and microbubble resonators (MBRs) have been extensively studied for pressure-sensing applications. Hollow spherical WGMRs made of PMMA offered the first proof of the feasibility of WGM-based pressure sensors.[111] Pressure tuning of an MBR was first demonstrated by Henze et al.;[119] the same authors also demonstrated laser tuning of a hollow microbottle by changing the pressure inside the bottle.[120] Another interesting example of a WGMR application in the field of physical sensors is provided by an acceleration sensor, based on the architecture that, in order to make easier and more efficient the coupling of light into WGMs, combines strip-line pedestal anti-resonant reflecting optical waveguides and a microsphere. The sensing method takes advantage of the variation of the coupling gap. The fiber stem that holds the microsphere acts as a flexure beam for the microresonator; when a force (provided by a piezoelectric shaker) is applied to the stem, the coupling gap changes, and the resonance properties change as well. Sensitivities better than 1 mg at 250-Hz bandwidth, with a noise floor of 100 μg, were demonstrated.[121] A miniature optical gyroscope based on a waveguide-coupled sequence of WGM microresonators was also proposed.[122] It was demonstrated that the composite structure would allow for several orders of magnitude enhancement, even though some practical problems remain to be faced: the coupling of many resonators to a single waveguide and achieving the same resonant frequency for all of them is not an easy task, and some individual trimming may be necessary.

Optomechanical coupling between optical WGMs and mechanical resonances is an alternative approach to measure forces. Sub-pg mass sensing has been demonstrated using a microtoroid WGMR.[114] An optomechanofluidic viscometer has been demonstrated by using an MBR and measuring the line broadening of the mechanical mode.[115] Han et al.[123] also demonstrated the potential use of MBRs as pressure sensors in a high-temperature environment. The underlying physical mechanism is that the pressure increment will increase the radius of the MBR and therefore change the mechanical frequency. Geometrical changes and stress would also modify the optical WGMs that, in turn, will change the laser power coupling and also modify the temperature. Because the mechanical modulus also depends on the temperature, the mechanical frequency will change, too. Figure 12 shows the aerostatic tuning mechanism.

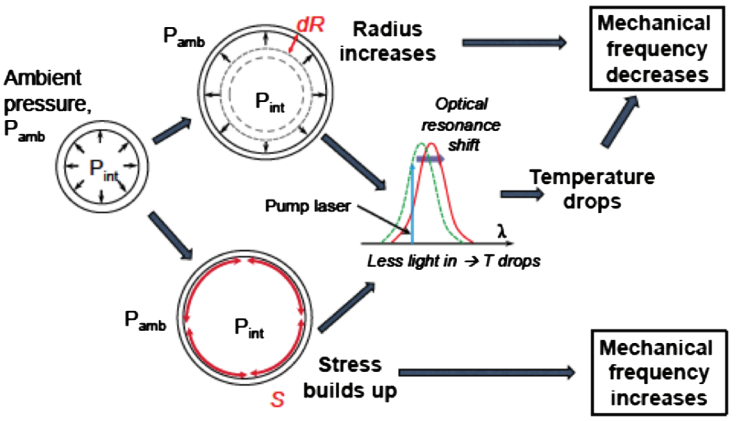

Figure 12 Sketch of the aerostatic tuning mechanism: the increment in pressure will modify the radius, and increase the stress (*S*), and it will shift the mechanical frequency through the optical mode shift. Reprinted with permission from Ref. 123.

5.2 Gas and biological sensors

Microspheres were first proposed as gas sensors in the pioneering papers by Rosenberger and Rezac.[124,125] The authors used a microspherical WGMR in the 1530- to 1580-nm spectral window to detect trace amounts of carbon dioxide, carbon monoxide, ammonia, and acetylene. The same group, some years later, published several papers on the broadband detection of gases.[126,127] The authors first locked the resonance and then controlled the changes in the dip depth (the contrast of the resonance); by this method, a detection limit around 1000 ppm was achieved. A very interesting strategy to produce ultra-sensitive WGM chemical (and possibly biochemical) sensors was suggested by Lin et al.,[128] based on the use of a zeolite coating on top of a silica microsphere. Zeolites are crystalline aluminosilicate materials with uniform sub-nanometer or nanometer scale pores; such pores can absorb chemical molecules of specific size from the environment efficiently and selectively. The authors developed a numerical model, based on the perturbation theory presented by Teraoka and Arnold,[129] showing that the effect of the zeolite layer can increase the sensitivity by nearly 2 orders of magnitude and that the sensing characteristic is linear in a wide range of refractive index changes. Figure 13 shows the proposed sensor.

Optical fluidic ring resonators (OFRRs—a more general definition than LCORRs, the latter being limited to liquids) were also proposed as gas sensors.[130] In this case, an OFRR, with a typical diameter of 75 μm, employs a thin-walled (around 4 μm) fused-silica capillary whose inner surface is coated by a gas-sensitive polymer. The coating's swelling and/or refractive index changes are different for each polymer–gas couple. The sensitivity increases with the coating thickness; as an example, according to simulations of a 200-nm-thick polymer layer,

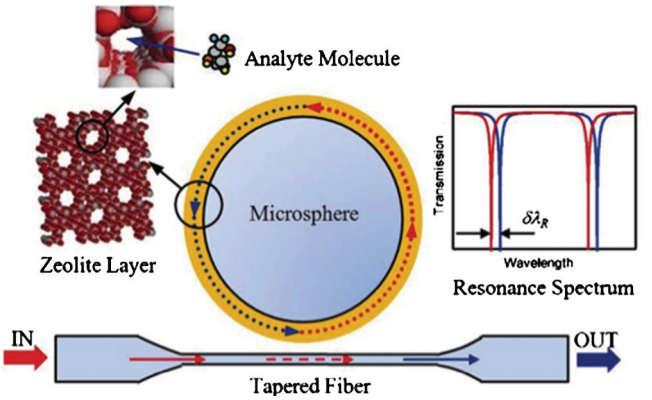

Figure 13 Proposed zeolite-coated microsphere sensor. Reprinted with permission from Ref. 128.

the sensitivity is 18 nm/RIU, corresponding to an LoD of 5.6×10^{-6} RIU; with a 1000-nm-thick coating, the sensitivity becomes 160 nm/RIU, resulting in a LoD of 6×10^{-7} RIU.[130]

Table 3 summarizes some of the main results obtained in gas sensing by using WGMRs.

Looking at biochemical sensing applications, it is easy to note that the use of WGMRs as optical transducers for biosensing has increased at a rapid pace since the seminal paper by Vollmer et al.,[135] where the feasibility of spherical WGMRs as label-free multiplexed sensors was demonstrated. We remind the reader that a sensor is defined as a biosensor only if it is capable of providing specific quantitative or semiquantitative analytical information using a biological recognition element (BRE), which is retained in direct spatial contact with a transduction element. Different biochemical receptors can act as a BRE, such as antibodies, streptavidin, aptamers, and enzymes; the corresponding analytes are antigens, biotin/biotinylated proteins, proteins, and amino acids.

Table 3 Gas sensing by WGMRs.

WGMR type and material	Gas detected	LoD	Ref.
Microsphere, silica	Atmospheric trace gas	1000 ppm	126
Microring, polymer sol-gel coating	Water vapor	16 pm/%RH	131
Microring, polymer coating	Isopropanol	50 ppm	132
Microring, SoI	Ammonia	0.4%	133
Microring, polymer sol-gel coating	Ethanol	1.13 pm/ppm	134
LCORR	Ethanol	200 ppm	130

Briefly, the optical mechanisms used for (bio)sensing rely either on changes of phase (refractive index), changes of amplitude (absorption), or changes of frequency (fluorescence, Raman, nonlinear optical phenomena). The phase and amplitude (adsorption) changes are a direct monitoring technique, whereas the frequency changes can also include an indicator or marker (labeled system). Fluorescence detection in biochemical sensing usually relies heavily on the use of a marked/labeled target, even if this is not always necessary, because there are plenty of proteins that are naturally fluorescent. Raman-based detection is unique since target molecules are not labeled but the detection system is based on Raman emitted light. The disadvantages of the labeled systems (higher cost and possibly reduced reactivity) are normally compensated by the lower LoD, whereas in the case of direct monitoring, the disadvantage lies in the ineffectiveness of detecting small-molecular-weight analytes and in the sensitivity to nonspecific binding. Figure 14 summarizes the different mechanisms involved in biochemical sensing by an optical WGMR.

Biosensors can also be classified by their assay format, the direct and indirect ones being the most common. Competitive assays represent a third format frequently used in labeled systems, where the target analyte has a small molecular weight. Figure 15 graphically illustrates the different formats commonly used in biosensing: sandwich, direct noncompetitive, and competitive (direct or indirect); here, reference is made to immunoassay (antibody–antigen) formats, but the same scheme is also valid for apta-assays (aptamers). Direct noncompetitive assays show a great potential but have a primary limitation: nonspecific binding of nontarget analytes. In the competitive assay, either the antibody is immobilized onto the surface and the antigen and labeled antigen compete for the available binding sites, or the antigen is immobilized onto the surface, and the antibody and the labeled antibody compete for the available binding sites. In the indirect

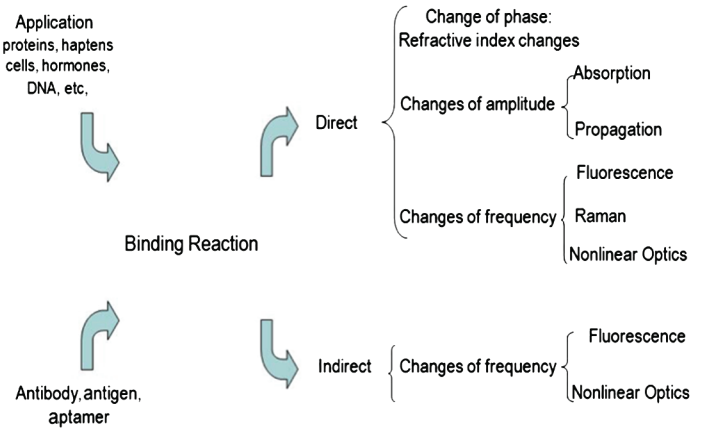

Figure 14 Optical transduction used in biosensors.

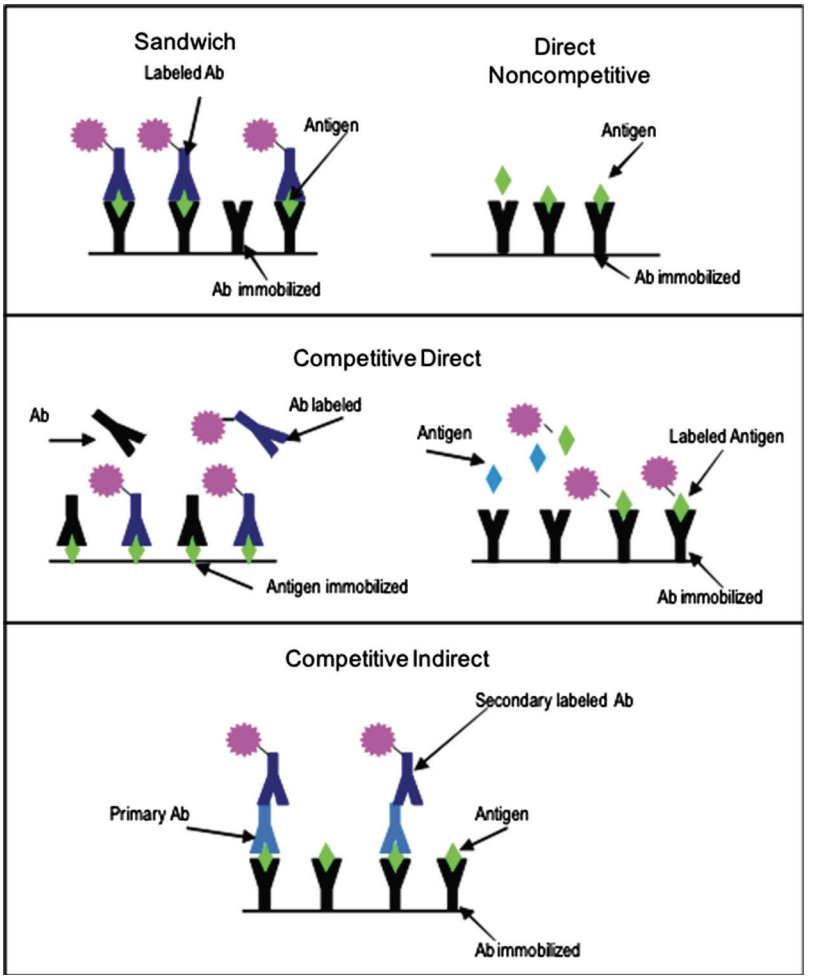

Figure 15 General immunoassays formats. (top) Noncompetitive direct sandwich format and direct noncompetitive format. (middle) Competitive direct assays: immobilized antigen and labeled antibody (Ab) or immobilized antibody and labeled antigen. (bottom) Competitive indirect assay: detection through a secondary labeled antibody.

competitive assay, the antibody bound to the antigen is detected through a secondary labeled antibody; in this case, the signal is directly proportional to the concentration of the analyte, either the antigen or the antibody. Competitive assays can be described using the following reaction:

$$\mathrm{Ab} + \mathrm{Ag} + \mathrm{Ag}^{*} \rightarrow \mathrm{AbAg} + \mathrm{AbAg}^{*},$$

where Ab is the antibody, Ag is the antigen, Ag* is the labeled antigen, AbAg is the antibody–antigen complex, and AbAg* is the antibody-labeled antigen complex. The transducer can differentiate the relative amount of antibody binding

sites that are occupied by the analyte: it results in a sensor signal that is inversely proportional to the analyte concentration. Competitive assays are very complex and time consuming because they are multi-stepped. To our knowledge, no competitive assay has ever been accomplished by using a WGMR as transducer, mainly because of the impossibility in this case to distinguish one photon fluorescence from the excitation laser.[136]

A new trend in WGMR sensing is the use of metal–dielectric hybrid WGMRs for sensitivity enhancement. Santiago-Cordoba et al.[137] combined the advantages of a NP-based assay (namely, large sensing area, rapid mixing with the analyte, and the possibility of extracting NPs from a complex sample for subsequent optical analysis) with the high sensitivity of a WGMR to determine the amount of protein bound to the NPs by analyzing the frequency shift of hybrid photonic-plasmonic modes. Figure 16 shows a sketch of the setup and the working principle of the device.

Placing the NPs directly onto the WGMR surface is a much more effective way of enhancing sensitivity, thus allowing one to detect single proteins[138] and single nucleic acid interactions.[10] In the former paper,[138] the authors demonstrated the detection of 0.11 ag of bovine serum albumin and 1 ag of a thyroid cancer marker, thyroglobulin. They claimed that the gold NPs had a rough surface with bumps the size of proteins, as sketched in Fig. 17, where the detection mechanism is also briefly depicted.

The high sensitivity and capability of a microbubble resonator to detect NPs, due to its optomechanical properties, can also be combined with a flow speed comparable to commercial flow cytometry.[139] Figure 18 shows a sketch of the working principle of long-range phonon-mediated sensing. The long-range

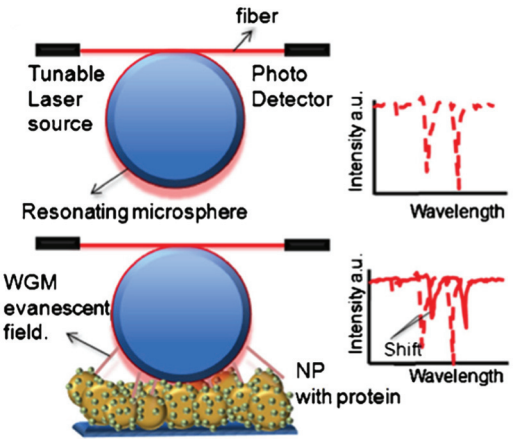

Figure 16 (top) A WGMR-coupling system in air and the transmission spectrum. (bottom) The WGMR in contact with NPs covered with protein, and the corresponding shift of the resonant peaks in the transmission spectrum. Reproduced with permission from Ref. 137.

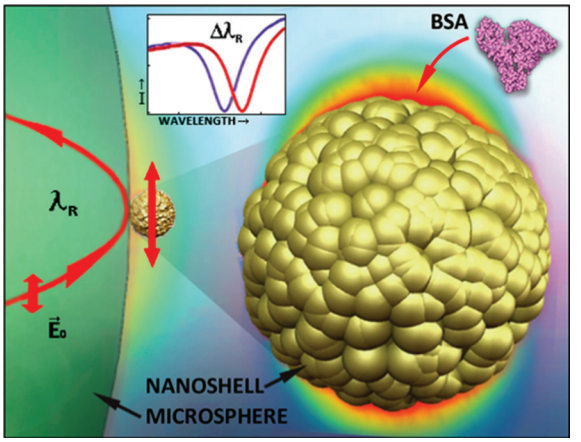

Figure 17 Rendered image of the detection mechanism of a hybrid WGMR consisting of a spherical WGMR and a gold NP. Reproduced with permission from Ref. 138 (Copyright 2013 American Chemical Society).

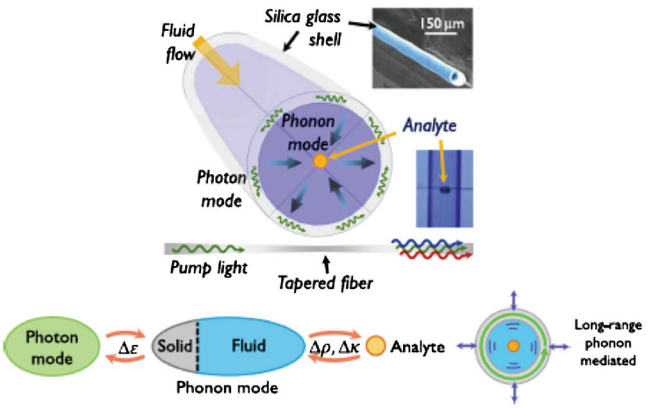

Figure 18 Optomechanical principle of detection of flowing particles. Reproduced and modified with permission from Ref. 139.

phonons extend across the solid shell of the MBR and the liquid phase inside the MBR. The optical WGM excites the mechanical modes (phonons) that penetrate the total volume of the fluid through radiation pressure and Brillouin scattering. The changes in the fluid determine a frequency shift of the mechanical mode.

Another approach to study the blood flow by a thin-film device, portable and suitable for *in situ* operation, has been recently proposed.[140] The device is based on a PANDA ring resonator structure, as sketched in Fig. 19, to be implemented in a nonlinear material, in order to exploit nonlinear optical phenomena.

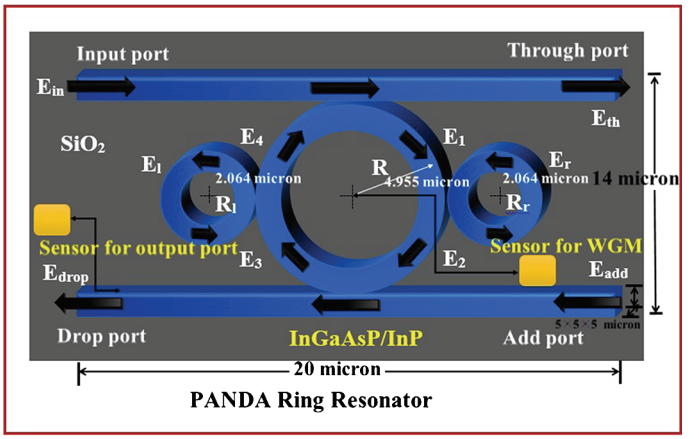

Figure 19 Sketch of a PANDA ring resonator, to be fabricated in a nonlinear optical material, such as InGaAsP/InP on top of a silica substrate. The size of the center ring and of the two side rings is indicated. Reproduced with OSA permission from Ref. 140.

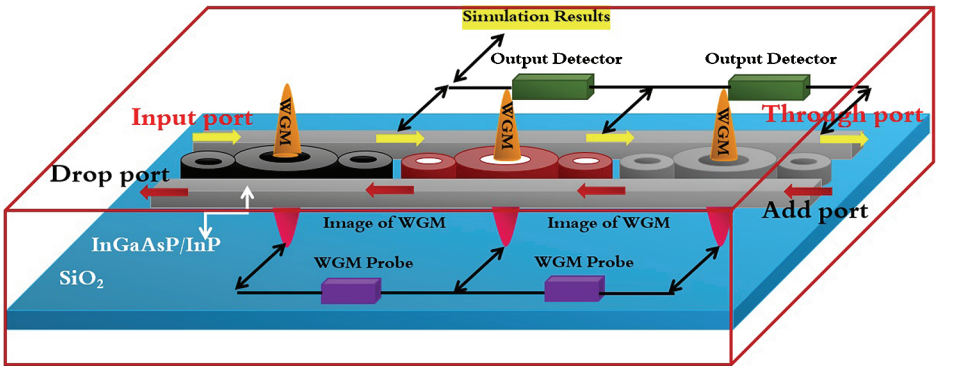

Figure 20 Sketch of a fluid sensing device using three nonlinear semiconductor PANDA ring resonators in series. The two WGM probes, generated by comparison between the different flow positions, give information on the flow rate. Reproduced with OSA permission from Ref. 140.

By using three PANDA resonators in series, as depicted in Fig. 20, it is possible to study the velocity of a fluid and, specifically, the blood flow rate in a patient. A 3-D WGM probe is also available due to the microconjugate mirror function.[141] Such a 3-D probe can penetrate into the blood vessel and its contents; the authors claim that the blood content can be analyzed within a few hundred micrometers in skin depth, which would be very useful for medical diagnosis.[140]

Given the growing interest in this area, Table 4 can only give an indicative, not exhaustive, summary of the most appealing results achieved; for more detailed information on WGMR biosensing, readers may refer to the published review papers.[1,4,11–15]

Table 4 WGMR biosensors.

WGMR type	Assay type	Functionalization technique	Analyte detected	LoD	Ref.
Microsphere, silica	Direct	Physical adsorption	Biotin	50 Da	57
Microsphere, silica	Direct	Covalent binding	DNA strands	Single mismatch	135
Microsphere, silica	Direct	Physical adsorption	Influenza A	Single virus	142
Microsphere, silica	Direct-aptamer	Covalent binding	Thrombin	Est. 1 NIH Unit/mL	58
Microsphere, silica	Direct-aptamer	Covalent binding	Thrombin and VEGF	40 nM	30
Microsphere, silica	Direct-enzyme	Covalent binding	Trypsin	10 pg/mL	143
Microsphere, silica	Direct-antibody	Covalent binding	Ovarian cancer biomarker	240 pg/mL	144
Microsphere, silica	Direct	Physical adsorption	Bacteria	100 cfu/mm^2	145
Microsphere, silica	Direct-aptamer	Covalent binding	Hg (II)	240 nm and 50 nM	146 and 147
LCORR, silica	Direct-antibody	Covalent binding	HER2 breast cancer biomarker	13 mg/mL	148
LCORR, silica	Direct	Covalent binding	CD4+ and CD8+ T-lymphocytes	200 cells/L CD4+ and 250 cells/L CD8+	149
LCORR, fluorescent	Direct	Physical adsorption	Neutravidin	33 nM	150
Microring, SoI	Direct-antibody	Covalent binding	CEA	25 ng/mL	151
Microring, SoI	Direct-antibody	Covalent binding	PSA, CEA, interleukin, AFP, TNF-alpha	100 pg/mL	152
Microring, SoI	Sandwich assay-antibody	Covalent binding	Interleukin-2	100 pg/mL	153
Racetrack, SiON	Direct-aptamer	Covalent binding	Aflatoxin M1	12.5 nM	41

Note: VEGF, vascular endothelial growth factor; PSA, prostate specific antibody; HER, human epidermal growth factor receptor; CEA, carcinoembryonic antigen; AFP, alpha-fetoprotein; and TNF-alpha, tumor necrosis factor.

6 Conclusions and Outlook

WGMR-based sensors have shown their enormous potential in physical, biomedical, and biochemical sensing applications, and they are, indeed, at the forefront of the research in these areas. However, there are still problems to be faced before going from the laboratory to the market: these problems have to be overcome in order to allow a wide exploitation of these devices. One of the main obstacles for all WGMR sensors concerns device integration; specificity, in biochemical and biomedical sensing, is another challenge. Two-dimensional WGMRs are suitable for planar integration and have multiplexing capabilities, but a simple and cheap protocol for full microfluidic integration, allowing fast response times, has yet to be demonstrated. The fabrication of 3-D WGMRs is, in principle, definitely cheaper, as they do not require film deposition processes and advanced photolithography; commercial mass fabrication of microspheres or microbubbles, however, is still very challenging. 3-D WGMRs, thus, are still far from portable, robust, reproducible, and user-friendly lab-on-chip devices; they rather keep being at the stage of chips in a lab. As to the specificity requirement, interesting perspectives concern the use of active sensors based on stimulated processes, such as Raman scattering and/or Brillouin scattering, in order to avoid functionalization procedures that may highly damage the Q-factor. Stimulated Raman scattering could also be used for molecular fingerprinting, as in surface-enhanced Raman scattering, where the WGMR sensor could substitute the plasmonic platform. Other approaches which deserve further investigation are those based on nonlinear optics, such as two-photon fluorescence excitation[136] of naturally fluorescent proteins (e.g., triptofan, collagen, etc.). Finally, the use of more-complex devices, for instance, involving plasmonic nanostructures (particles, shells, rods, etc.) deposited on the surface of (or coupled to) a microresonator, opens the way not only to a strong enhancement of the sensitivity but also to a greater capability of manipulating the local environment.

7 Acknowledgments

The colleagues at IFAC CNR (Sesto Fiorentino, Italy), IFN CNR (Trento, Italy), Ruder Boskovic Institute (Zagreb, Croatia), and ENSSAT (Lannion, France) are gratefully acknowledged for their long-lasting collaboration and fruitful discussions.

References

1. G. Righini et al., "Whispering gallery mode microresonators: fundamentals and applications," *Riv. Nuovo Cimento* **34**, 435 (2011). DOI: 10.1393/ncr/i2011-10067-2
2. K. J. Vahala, "Optical microcavities," *Nature* **424**, 839–846 (2003).
3. J. Ward and O. Benson, "WGM microresonators: sensing, lasing and fundamental optics with microspheres," *Laser Photonics Rev.* **5**(4), 553–570 (2011).

4. A. Chiasera et al., "Spherical whispering-gallery-mode microresonators," *Laser Photonics Rev.* **4**, 457–482 (2010).
5. M. V. Maximov et al., "Ultrasmall microdisk and microring lasers based on InAs/InGaAs/GaAs quantum dots," *Nanoscale Res. Lett.* **9**, 657 (2014).
6. J. Lim et al., "Chasing the thermodynamic noise limit in microcavity lasers," in *Frontiers in Optics*, *Optical Society of America* (2015).
7. X. Yi et al., "Theory and measurement of the soliton self-frequency shift and efficiency in optical microcavities," *Opt. Lett.* **41**, 3419 (2016).
8. F. H. Suhailin et al., "Kerr nonlinear switching in a hybrid silica silicon microspherical resonator," *Opt. Express* **23**, 17263 (2015).
9. P.-B. Li, S.-Y. Gao, and F.-L. Li, "Quantum information transfer with nitrogen-vacancy centers coupled to a whispering-gallery microresonator," *Phys. Rev. A* **83**, 054306 (2011).
10. M. D. Baaske, M. R. Foreman, and F. Vollmer, "Single-molecule nucleic acid interactions monitored on a label-free microcavity biosensor platform," *Nat. Nanotechnol.* **9**, 933–939 (2014).
11. F. Vollmer and S. Arnold, "Whispering-gallery-mode biosensing: label-free detection down to single molecules," *Nat. Methods* **5**, 591–596 (2008).
12. S. Soria et al., "Optical microspherical resonators for biomedical sensing," *Sensors* **11**, 785–805 (2011).
13. M. R. Foreman, J. D. Swaim, and F. Vollmer, "Whispering gallery mode sensors," *Adv. Opt. Photonics* **7**, 168–240 (2015).
14. G. C. Righini and S. Soria, "Biosensing by WGM micro spherical resonators," *Sensors* **16**(6), 905 (2016).
15. G. Nunzi Conti, S. Berneschi, and S. Soria, "Aptasensors based on whispering gallery mode resonators," *Biosensors* **6**(3), 28 (2016).
16. D. Vernooy et al., "Cavity QED with high-Q whispering gallery modes," *Phys. Rev. A* **57**, R2293–R2296 (1998).
17. A. Rasoloniaina et al., "Controlling the coupling properties of active ultrahigh-Q WGM microcavities from undercoupling to selective amplification," *Sci. Rep.* **4**, 4023 (2014). doi:10.1038/srep04023
18. G. Mie, "Beitung zur optik trüber melien, speziell kolloïdaler metallosungen," *Ann. Phys.* **330**, 377–445 (1908).
19. L. Rayleigh, "The problem of the whispering gallery," *Philos. Mag.* **20**(120), 1001–1004 (1910).
20. B. R. Johnson, "Theory of morphology-dependent resonances: shape resonances and width formulas," *J. Opt. Soc. Am. A* **10**(2), 343 (1993).
21. S. Arnold et al., "Microparticle photophysics illuminates viral bio-sensing," *Faraday Discuss.* **137**, 65–83 (2008).
22. A. N. Oraevsky, "Whispering-gallery waves," *IEEE J. Quantum Electron.* **32**(5), 377–400 (2002).
23. M. R. Foreman et al., "Enhanced nanoparticle detection with liquid droplet resonator," *Eur. Phys. J. Spec. Top.* **223**, 1971–1988 (2014).
24. M. Gorodetsky, A. Savchenkov, and V. Ilchenko, "Ultimate Q of optical microsphere resonators," *Opt. Lett.* **21**, 453–455 (1996).
25. L. Maleki, V. S. Ilchenko, A. A. Savchenkov, and A. B. Matsko, "Crystalline Whispering Gallery Mode Resonators in Optics and Photonics," Chapter 3 in *Practical Applications of Microresonators in Optics and Photonics*, 133–209, dA. Matsko, Ed., Taylor and Francis, Boca Raton, FL (2009).
26. D. Weiss et al., "Splitting of high-Q Mie modes induced by light backscattering in silica microspheres," *Opt. Lett.* **20**, 1835–1837 (1995).

27. J. Zhu et al., "On-chip single nanoparticle detection and sizing by mode splitting in an ultrahigh-Q microresonator," *Nat. Photonics* **4**, 46–49 (2010).
28. G. Nunzi Conti et al., "Coupling approaches and new geometries in whispering-gallery-mode resonators," *Proc. SPIE* **8236**, 82360V (2012).
29. G. Righini et al., "Whispering gallery mode resonators for microlasers and microsensors," *Proc. SPIE* **6029**, 602903 (2006).
30. L. Pasquardini et al., "Whispering gallery modes aptasensors for detection of blood proteins," *J. Biophotonics* **6**, 178–187 (2013).
31. A. O'Keefe and D. A. Deacon, "Cavity ring-down optical spectrometer for absorption measurements using pulsed laser sources," *Rev. Sci. Instrum.* **59**, 2544–2551 (1988).
32. G. Berden, R. Peeters, and G. Meijer, "Cavity ring-down spectroscopy: experimental schemes and applications," *Int. Rev. Phys. Chem.* **19**(4), 565–607 (2000).
33. S. Lin, E. Schonbrun, and K. Crozier, "Optical manipulation with planar silicon microring resonators," *Nano Lett.* **10**(7), 2408–2411 (2010).
34. J.-B. Jager et al., "High Q silica microcavities on a chip: from microtoroid to microsphere," *Appl. Phys. Lett.* **99**, 181123 (2011).
35. A. Yalcin et al., "Optical sensing of biomolecules using microring resonators," *IEEE J. Sel. Top. Quantum Electron.* **12**, 148–155 (2006).
36. E. Krioukov et al., "Sensor based on an integrated optical microcavity," *Opt. Lett.* **27**, 512–514 (2002).
37. M. Iqbal et al., "Label-free biosensor arrays based on silicon ring resonators and high-speed optical scanning instrumentation," *IEEE J. Sel. Top. Quantum Electron.* **16**, 654–661 (2010).
38. C.-Y. Chao, W. Fung, and L. Guo, "Polymer microring resonators for biochemical sensing applications," *IEEE J. Sel. Top. Quantum Electron.* **12**, 134–142 (2006).
39. N. Lin et al., "Thermostable refractive index sensors based on whispering gallery modes in a microsphere coated with poly(methyl methacrylate)," *Appl. Opt.* **50**, 992–998 (2011).
40. P. Girault et al., "Racetrack micro-resonators based on ridge waveguides made of porous silica," *Opt. Mater.* **50**, 167–174 (2015).
41. R. Guider et al., "Design and optimization of SiON ring resonator-based biosensors for aflatoxin M1 detection," *Sensors* **15**, 17300–17312 (2015).
42. T. Beck et al., "High-Q polymer resonators with spatial controlled photo-functionalization for biosensing applications," *Appl. Phys. Lett.* **102**, 121108 (2013).
43. D. Gandolfi et al., "Role of edge inclination in an optical microdisk resonator for label-free sensing," *Sensors* **15**, 4796–4809 (2015).
44. J. Flueckiger et al., "Sub-wavelength grating for enhanced ring resonator biosensor," *Opt. Express* **24**, 15672–15686 (2016).
45. S. Mitatha et al., "Optical vortices generated by light pulses within a Panda ring resonator," *J. Nonlinear Opt. Phys. Mater.* **20**(1), 85–97 (2011).
46. M.-C. Tien et al., "Ultra-high quality factor planar Si_3N_4 ring resonators on Si substrates," *Opt. Express* **19**, 13551–13556 (2011).
47. M. Soltani, S. Yegnanarayanan, and A. Adibi, "Toward ultimate miniaturization of high Q silicon traveling-wave microresonators," *Opt. Express* **18**, 19541–19557 (2010).
48. A. Ramachandran et al., "A universal biosensing platform based on optical micro-ring resonators," *Biosens. Bioelectron.* **23**, 939–944 (2008).
49. A. A. Savchenkov et al., "Kilohertz optical resonances in dielectric crystal cavities," *Phys. Rev. A* **70**, 051804 (2004).
50. L. Maleki and A. B. Matsko, "Lithium niobate whispering gallery mode resonators: applications and fundamental studies," in *Ferroelectric Crystals for Photonics Applications*, 337–383, P. Ferraro, S. Grilli, and P. De Natale, Eds., Springer-Verlag, Berlin Heidelberg (2009).

51. G. Nunzi Conti et al., "Planar coupling to high-Q lithium niobate disk resonators," *Opt. Express* **19**(4), 3651 (2011).
52. J. Lin et al., "Fabrication of high-Q lithium niobate microresonators using femtosecond laser micromachining," *Sci. Rep.* **5**, 8072 (2015).
53. J. Wang et al., "High-Q lithium niobate microdisk resonators on a chip for efficient electro-optic modulation," *Opt. Express* **23**(18), 23072–23078 (2015).
54. D. K. Armani et al., "Ultra-high-Q toroid microcavity on a chip," *Nature* **421**, 925–928 (2003).
55. X.-F. Liu et al., "Fabrication of a microtoroidal resonator with picometer precise resonant wavelength," *Opt. Lett.* **41**(15), 3603–3606 (2016).
56. J. Su, A. F. Goldberg, and B. M. Stoltz, "Label-free detection of single nanoparticles and biological molecules using microtoroid optical resonators," *Light* **5**, e16001 (2016).
57. F. Vollmer et al., "Protein detection by optical shift of a resonant microcavity," *Appl. Phys. Lett.* **80**, 4057–4059 (2002).
58. H. Zhu et al., "Aptamer based microsphere biosensor for thrombin detection," *Sensors* **6**, 785–795 (2006).
59. M. Brenci et al., "Microspherical resonators for biophotonic sensors," *Proc. SPIE* **6158**, 61580S (2006).
60. D. Farnesi et al., "Stimulated anti-stokes Raman scattering resonantly enhanced in silica microspheres," *Opt. Lett.* **39**(20), 5993 (2014).
61. H. Tzeng et al., "Laser-induced shape distortions of flowing droplets deduced from morphology-dependent resonances in fluorescence spectra," *Opt. Lett.* **10**, 209–211 (1985).
62. A. Campillo, J. Eversole, and H. Lin, "Cavity quantum electrodynamics enhancement of stimulated emission in microdroplets," *Phys. Rev. Lett.* **67**, 437–440 (1991).
63. Y. F. Yu et al., "Sandwiched droplet resonator for low concentration protein detection," in *IEEE Conf. Proc.—PhotonicsGlobal*, Singapore, pp. 1–2 (2008).
64. I. M. White et al., "Integrated multiplexed biosensors based on liquid core optical ring resonators and antiresonant reflecting optical waveguides," *Appl. Phys. Lett.* **89**, 191106 (2006).
65. X. Fan et al., "Overview of novel integrated optical ring resonator bio/chemical sensors," *Proc. SPIE* **6452**, 64520M (2007).
66. M. Sumetsky et al., "Optical liquid ring resonator sensor," *Opt. Express* **15**(22), 14376–14381 (2007).
67. V. Zamora et al., "Refractometric sensor based on whispering gallery modes of thin capillaries," *Opt. Express* **15**(19), 12011–12016 (2007).
68. V. Zamora et al., "Cylindrical optical microcavities: basic properties and sensor applications," *Photonics Nanostruct. Fundam. Appl.* **9**(2), 149–158 (2010).
69. J. D. Suter et al., "Label-free quantitative DNA detection using the liquid core optical ring resonator," *Biosens. Bioelectron.* **23**, 1003–1009 (2008).
70. M. Sumetsky, "Whispering-gallery-bottle microcavities: the three-dimensional etalon," *Opt. Lett.* **29**, 8–10 (2004).
71. M. Sumetsky, Y. Dulashko, and R. S. Windeler, "Optical microbubble resonator," *Opt. Lett.* **35**, 898–900 (2010).
72. P. Bianucci, "Optical microbottle resonators for sensing," *Sensors* **16**(11), 1841 (2016).
73. S. Berneschi et al., "High Q silica microbubble resonators fabricated by arc discharge," *Opt. Lett.* **36**(17), 3521–3523 (2011).
74. A. Cosci et al., "Confocal reflectance microscopy for determination of microbubble resonator thickness," *Opt. Express* **23**(13), 16693–16701 (2015).
75. Y. Yang et al., "High-Q, ultrathin-walled microbubble resonator for aerostatic pressure sensing," *Opt. Express* **24**(1), 294–299 (2016).

76. Y. Wang et al., "A review of droplet resonators: operation method and application," *Opt. Laser Technol.* **86**, 61–68 (2016).
77. J. Haase et al., "Hemispherical resonators with embedded nanocrystal quantum rod emitters," *Appl. Phys. Lett.* **97**, 211101 (2010).
78. V. D. Ta et al., "Application of self-assembled hemispherical microlasers as gas sensors," *Appl. Phys. Lett.* **102**, 031107 (2013).
79. M. Sumetsky, Y. Dulashko, and R. S. Windele, "Super free spectral range tunable optical microbubble resonator," *Opt. Lett.* **35**, 1866–1868 (2010).
80. P. Schiavone et al., "Thermal nanoimprint fabrication of silicon high Q optical microdisk resonators," in *23rd Annual Meeting of the IEEE Photonics Society*, pp. 417–418 (2010).
81. G. Kim and J. H. Shin, "Luminescent silicon-rich nitride horizontal air-slot microdisk resonators for biosensing," *IEEE Photonics Technol. Lett.* **28**(21), 2331–2334 (2016).
82. A. Dousse et al., "Scalable implementation of strongly coupled cavity-quantum dot devices," *Appl. Phys. Lett.* **94**, 121102 (2009).
83. G. S. Solomon, M. Pelton, and Y. Yamamoto, "Single-mode spontaneous emission from a single quantum dot in a three-dimensional microcavity," *Phys. Rev. Lett.* **86**(17), 3903–3906 (2001).
84. W. Bogaerts et al., "Silicon microring resonators," *Laser Photonics Rev.* **6**(1), 47–73 (2012).
85. K. Miura, K. Tanaka, and K. Hirao, "Laser oscillation on both the $4F_{3/2}$–$4I_{11/2}$ et $4F_{3/2}$–$4I_{13/2}$ transitions on Nd3+ ions using a fluoride glass microsphere," *J. Non-Cryst. Solids* **213–214**, 276–280 (1997).
86. X. Peng et al., "Fiber-taper-coupled L-band Er3+-doped tellurite glass microsphere laser," *Appl. Phys. Lett.* **82**, 1497–1499 (2003).
87. G. Nunzi Conti et al., "Spectroscopic and lasing properties of Er3+-doped glass microspheres," *J. Non-Cryst. Solids* **352**, 2360–2363 (2006).
88. G. C. Righini et al., "Er3+-activated sol-gel silica derived spherical microresonators," *Glass Technol. Eur. J. Glass Sci. Technol. Part A* **48**, 200–203 (2007).
89. S. Grilli et al., "3D lithography by rapid curing of the liquid instabilities at nanoscale," *Proc. Natl. Acad. Sci. U. S. A.* **108**(37), 15106–15111 (2011).
90. Y. Yamamoto, "Spherical resonators from conjugated polymers," *Polym. J.* **48**, 1045–1050 (2016).
91. A. J. Maker and A. M. Armani, "Fabrication of silica ultra high quality factor microresonators," *J. Vis. Exp.* **65**, e4164 (2012). doi: 10.3791/4164
92. J. Yao et al., "Silicon microtoroidal resonators with integrated MEMS tunable coupler," *IEEE J. Sel. Top. Quantum Electron.* **13**(2), 202–208 (2007).
93. M. Ilchenko et al., "Microtorus: a high-finesse microcavity with whispering-gallery modes," *Opt. Lett.* **26**(5), 256–258 (2001).
94. Y. Tanushi, M. Wake, and S. Yokoyama, "Design and fabrication of race-track optical ring resonator," in *Proc. 1st Progress Report COE21*, Vol. **1**, pp. 152–153 (2004).
95. M. Balakrishnan et al., "Fabrication of an electro-optic polymer microring resonator," in *Proc. Symp. IEEE/LEOS Benelux*, pp. 73–76 (2006).
96. S. Arnold et al., "Shift of whispering gallery modes in microspheres by protein adsorption," *Opt. Lett.* **28**, 272 (2003).
97. I. Teraoka and S. Arnold, "Estimation of surface density of molecules adsorbed on a whispering gallery mode resonator: utility of isotropic polarizability," *J. Appl. Phys.* **102**, 076109 (2007).
98. I. Teraoka and S. Arnold, "Dielectric property of particles at interface in random sequential adsorption and its application to whispering gallery mode resonance-shift sensors," *J. Appl. Phys.* **101**, 023505 (2007).
99. I. Teraoka, S. Arnold, and F. Vollmer, "Perturbation approach to resonance shifts of whispering-gallery modes in a dielectric microsphere as a probe of a surrounding medium," *J. Opt. Soc. Am. B* **20**(9), 1937–1946 (2003).

100. I. Teraoka and S. Arnold, "Theory of resonance shifts in TE and TM whispering gallery modes by nonradial perturbations for sensing applications," *J. Opt. Soc. Am. B* **23**, 1381 (2006).
101. S. Arnold, S. Shopova, and S. Holler, "Whispering gallery mode bio-sensor for label-free detection of single molecules: thermo-optic vs. reactive mechanism," *Opt. Express* **18**, 281–287 (2010).
102. T. Le et al., "Optical resonant sensors: a method to reduce the effect of thermal drift," *Appl. Opt.* **48**, 458–463 (2009).
103. S. Arnold et al., "Whispering gallery mode carousel a photonic mechanism for enhanced nanoparticle detection in biosensing," *Opt. Express* **17**, 6230–6238 (2009).
104. J. Knittel et al., "Interferometric detection of mode splitting for whispering gallery mode biosensors," *Appl. Phys. Lett.* **97**(12), 123704 (2010).
105. L. Shao et al., "Detection of single nanoparticles and lentiviruses using microcavity resonance broadening," *Adv. Mater.* **25**, 5616–5620 (2013).
106. M. R. Foreman, W. L. Jin, and F. Vollmer, "Optimizing detection limits in whispering gallery mode biosensing," *Opt. Express* **22**(5), 5491–5511 (2014).
107. C. H. Dong et al., "Fabrication of high-Q polydimethylsiloxane optical microspheres for thermal sensing," *Appl. Phys. Lett.* **94**(23), 231119 (2009).
108. B.-B. Li et al., "On chip, high sensitivity thermal sensor based on high-Q polydimethylsiloxane-coated microresonator," *Appl. Phys. Lett.* **96**, 251109 (2010).
109. L. Xu et al., "High-Q silk fibroin whispering gallery microresonator," *Opt. Express* **24**(18), 20825–20830 (2016).
110. T. Tang et al., "Packaged optofluidic microbubble resonators for optical sensing," *Appl. Opt.* **55**, 395–399 (2016).
111. T. Ioppolo and M. V. Otugen, "Pressure tuning of whispering gallery mode resonators," *J. Opt. Soc. Am. B* **24**, 2721–2726 (2007).
112. T. Ioppolo et al., "Micro-optical force sensor concept based on whispering gallery mode resonators," *Appl. Opt.* **47**(16), 3009–3014 (2008).
113. J. Ward, N. Dhasmana, and S. N. Chormaic, "Hollow core whispering gallery resonator sensors," *Eur. Phys. J. Spec. Top.* **223**, 1917–1935 (2014).
114. F. Lu et al., "Sub-pg mass sensing and measurement with an optomechanical sensor," *Opt. Express* **21**(17), 19555–19567 (2013).
115. K. Han, K. Zhu, and G. Bahl, "Opto-mechano-fluidic viscometer," *Appl. Phys. Lett.* **105**, 014103 (2014).
116. Y.-Z. Yan et al., "Packaged silica microsphere-taper coupling system for robust thermal sensing applications," *Opt. Express* **19**, 5753–5759 (2011).
117. A. B. Petermann et al., "All-polymer whispering gallery mode sensor system," *Opt. Express* **24**(6), 6052–6062 (2016).
118. M. Himmelhaus and A. Francois, "In vitro sensing of biomechanical forces in live cells by a whispering gallery mode biosensor," *Biosens. Bioelectron.* **25**, 418–427 (2009).
119. R. Henze et al., "Tuning whispering gallery modes using internal aerostatic pressure," *Opt. Lett.* **36**(23), 4536–4538 (2011).
120. R. Madugani et al., "Linear laser tuning using a pressure-sensitive microbubble resonator," *IEEE Photonics Technol. Lett.* **28**, 1134–1137 (2016).
121. J. P. Laine et al., "Acceleration sensor based on high-Q optical microsphere resonator and pedestal anti resonant reflecting waveguide coupler," *Sens. Actuators A* **93**, 1–7 (2001).
122. A. B. Matsko et al., "Interference effects in lossy resonator chains," *J. Mod. Opt.* **51**(16–18), 2515–2522 (2004).
123. K. Han, J. Kim, and G. Bahl, "Aerostatically tunable optomechanical oscillators," *Opt. Express* **22**(2), 1267–1276 (2014).

124. A. Rosenberger and J. Rezac, "Evanescent wave sensor using microsphere whispering gallery modes," *Proc. SPIE* **3930**, 186–192 (2000).
125. A. T. Rosenberger and J. Rezac, "Whispering-gallery-mode evanescent wave microsensor trace gas detection," *Proc. SPIE* **4265**, 102–112 (2001).
126. G. Farca, S. I. Shopova, and A. Rosenberger, "Cavity-enhanced laser absorption spectroscopy using microresonator whispering-gallery modes," *Opt. Express* **15**, 17443 (2007).
127. S. Westcott et al., "Broadband optical absorbance spectroscopy using a whispering gallery mode microsphere resonator," *Rev. Sci. Instrum.* **79**, 033106 (2008).
128. N. Lin et al., "Ultrasensitive chemical sensors based on whispering gallery modes in a microsphere coated with zeolite," *Appl. Opt.* **49**, 6463–6471 (2010).
129. I. Teraoka and S. Arnold, "Whispering-gallery modes in a microsphere coated with a high-refractive index layer: polarization-dependent sensitivity enhancement of the resonance-shift sensor and TE TM resonance matching," *J. Opt. Soc. Am. B* **24**, 653–659 (2007).
130. Y. Sun et al., "Rapid chemical-vapor sensing using optofluidic ring resonators," *Opt. Lett.* **33**, 788–790 (2008).
131. B. Bhola et al., "Sol-gel based integrated optical microring resonator humidity sensor," *IEEE Sens. J.* **9**(7), 740–747 (2009).
132. A. Ksendzov, M. Homer, and A. Manfreda, "Integrated optics ring-resonator chemical sensor with polymer transduction layer," *Electron. Lett.* **40**, 63–65 (2004).
133. V. Passaro, F. Dell'Olio, and F. DeLeonardis, "Ammonia optical sensing by microring resonators," *Sensors* **7**, 2741–2749 (2007).
134. F. Pang et al., "Sensitivity to alcohols of a planar waveguide ring resonator fabricated by a sol-gel method," *Sens. Actuators B* **120**, 610–614 (2007).
135. F. Vollmer et al., "Multiplexed DNA quantification by spectroscopic shift of two microsphere cavities," *Biophys. J.* **85**, 1974–1979 (2003).
136. C. Pastells et al., "Two photon versus one photon fluorescence excitation in whispering gallery mode microresonators," *J. Lumin.* **170**, 860–865 (2016).
137. M. Santiago-Cordoba et al., "Nanoparticle-based protein detection by optical shift of a resonant microcavity," *Appl. Phys. Lett.* **99**, 073701 (2011).
138. V. R. Dantham et al., "Label-free detection of single protein using a nanoplasmonic-photonic hybrid microcavity," *Nano Lett.* **13**, 3347–3351 (2013).
139. K. Han, J. Kim, and G. Bahl, "High-throughput sensing of freely flowing particles with optomechanofluidics," *Optica* **3**(6), 585–591 (2016).
140. P. Phatharacorn, S. Chiangga, and P. Yupapin, "Analytical and simulation results of a triple micro whispering gallery mode probe system for a 3D blood flow rate sensor," *Appl. Opt.* **55**(33), 9504–9513 (2016).
141. S. Punthawanunt, P. P. Yupapin, and P. Phatharacorn, "Novel design of 3D imaging pixel on-chip using a microconjugate mirror system," *Nano Biomed. Eng.* **7**(2), 52–61 (2015).
142. F. Vollmer, S. Arnold, and D. Keng, "Single virus detection from the reactive shift of a whispering-gallery mode," *Proc. Natl. Acad. Sci. U. S. A.* **105**, 20701–20704 (2008).
143. N. M. Hanumegowda et al., "Label-free protease sensors based on optical microsphere resonators," *Sens. Lett.* **3**, 315–319 (2005).
144. H. Huckabay and R. C. Dunn, "Whispering gallery mode imaging for multiplexed detection of biomarkers," *Sens. Actuators B* **160**, 1262–1267 (2011).
145. H.-C. Ren et al., "High-Q microsphere biosensor—analysis for adsorption of rod like bacteria," *Opt. Express* **15**, 17410–17423 (2007).
146. N. M. Hanumegowda, I. White, and X. Fan, "Aqueous mercuric ion detection with microsphere optical ring resonator sensors," *Sens. Actuators B* **120**, 207–212 (2006).

147. F. Wu et al., "Integrating a DNA strand displacement reaction with a whispering gallery mode sensor for label-free mercury (II) ion detection," *Sensors* **16**, 1197 (2016).
148. J. Gohring, P. Dale, and X. Fan, "Detection of HER2 breast cancer biomarker using the opto-fluidic ring resonator biosensor," *Sens. Actuators B* **146**, 226–230 (2010).
149. J. Gohring and X. Fan, "Label free detection of QCD4+ and CD8+ T cells using the optofluidic ring resonator," *Sensors* **10**, 5798–5808 (2010).
150. S. Lane et al., "Protein biosensing with fluorescent microcapillaries," *Opt. Express* **23**(3), 2577–2590 (2015).
151. A. Washburn et al., "Label-free quantitation of a cancer biomarker in complex media using silicon photonic microring resonators," *Anal. Chem.* **81**, 9499–9506 (2009).
152. A. L. Washburn et al., "Quantitative, label-free detection of five protein biomarkers using multiplexed arrays of silicon photonic microring resonators," *Anal. Chem.* **82**(1), 69–72 (2010).
153. W. W. Shia and R. C. Bailey, "Single domain antibodies for the detection of ricin using silicon photonic microring resonator arrays," *Anal. Chem.* **85**, 805–810 (2013).

Giancarlo C. Righini is now a research associate (emeritus) at both the Enrico Fermi Center in Rome, Italy, and the Nello Carrara Institute of Applied Physics (IFAC CNR) in Sesto Fiorentino. He was a research director at IFAC, director of the Materials and Devices Department at CNR, and director of the Enrico Fermi Center. He was a vice-president of IUPAP and ICO. As a physicist, he has always worked in experimental optics and photonics, with interests in holography, fiber and integrated optics, optical materials, and optical sensors. He is the author of some 500 scientific papers (source: Web of Science) and has edited several books and conference proceedings; he has been on the editorial board of several journals. He is a chair of the TC20 Committee (Glasses for Optoelectronics) of ICG. He is a fellow member of EOS, OSA, SIOF, SPIE, and meritorious member of SIF (the Italian Physical Society).

Silvia Soria holds her M.Sc. and Ph.D. degrees in physics from the University of Barcelona in Spain. Previously, she worked at Laser Laboratorium Goettingen e.V., in Germany, at the ICFO-Institute of Photonics Science in Barcelona, Spain, and at the Enrico Fermi Center in Rome. Currently, she is a permanent researcher at IFAC–CNR (Nello Carrara Institute of Applied Physics, National Research Council, Italy). Her areas of research include lasers, nonlinear optics, soft matter, and optical sensing. She has authored over 50 papers and presented her results in many international congresses.